On Sounding in Wideband Channels

by

Sheng Jing

Submitted to the Department of Electrical Engineering and Computer Science
in partial fulfillment of the requirements for the degree of

Master of Science

at the

MASSACHUSETTS INSTITUTE OF TECHNOLOGY

June 2006

Author .....
Department of Electrical Engineering and Computer Science
June 9, 2006

Certified by .....
Lizhong Zheng
Assistant Professor
Thesis Supervisor

Certified by .....
Muriel Médard
Esther and Harold Edgerton Associate Professor
Thesis Supervisor

Accepted by .....
Arthur C. Smith
Chairman, Department Committee on Graduate Students

On Sounding in Wideband Channels

by

Sheng Jing

Submitted to the Department of Electrical Engineering and Computer Science
on June 9, 2006, in partial fulfillment of the
requirements for the degree of
Master of Science

Abstract

For an average-power-constrained wideband fading channel, on the one hand, if the transmitter has perfect knowledge of the fading state over the entire spectrum, the maximum achievable rate (Capacity) is infinite; on the other hand, if the transmitter has no knowledge of the channel's fading state, the capacity is finite. Therefore, the transmitter's knowledge of channel fading states has a great impact on the channel capacity. However, in the low SNR scenario, the energy per degree of freedom does not suffice to provide an accurate measurement of the channel over the entire spectrum in wideband channels. In the presence of feedback, we may garner information at the transmitter about some aspects of the channel quality over certain portion of the spectrum. In this work, we investigate a scheme to capture the effect of such information. We consider channel sounding with a finite amount of energy over a block-fading channel in both time and frequency. The quality of each subchannel is assessed as being the crossover probability in a BSC. In order to characterize a judicious policy for allocating energy to different subchannels in view of establishing their usefulness for transmission, we use a multi-armed bandit approach. This approach provides us with a cohesive framework to consider the relative costs and benefits of allotting energy for sounding versus transmission, and for repeated sounding of a single channel versus sounding of various different channels. In particular, we are able to give both an upper bound and a lower bound on the number of subchannels that should be probed for capacity maximization in terms of the available transmission energy, the available bandwidth and the fading characteristics of the channel. Moreover, the two bounds are so close to each other that they may well be treated as an approximation to the desirable number of subchannels to probe.

Thesis Supervisor: Lizhong Zheng
Title: Assistant Professor

Thesis Supervisor: Muriel Médard
Title: Esther and Harold Edgerton Associate Professor

Acknowledgments

I would like to thank my supervisors, Prof. Lizhong Zheng and Prof. Muriel Médard, for their insightful guidance and continuous support. I deeply acknowledge Prof. Zheng for his patience when I am slowly catching up with his pace of thinking. I am indebted to Prof. Médard for her numerous inspiring advice and invaluable care throughout the past two years.

I would like to thank my academic advisor, Prof. Munther A. Dahleh, for his careful guidance towards the finishing line of my master degree.

I would like to thank my friends at LIDS, partially including Shashibhushan P Borade, Emmanuel Abbe, Baris Nakiboglu, Chung Chan, Siddharth Ray, Wee Peng Tay, Yonggang Wen, Jianlong Tan, Fang Zhao, Yingzong Huang, Xin Huang, Jay Kumar Sundararajan, Cheng Luo, Jun Sun.

Special thanks go to my parents and Yi Wu, for the important place you hold in my life.

Contents

List of Figures

Chapter 1

Introduction

The growing popularity of mobile wireless communication applications makes it important to study the wireless fading channels. Meanwhile, wireless communications are increasingly carried out over a large bandwidth to meet the growing demand for higher data rates of the emerging new wireless applications (like video streaming). Moreover, as the energy consumption becomes critical, power-constraint communication and energy efficient communication schemes are desirable. Therefore, investigating wideband fading channels under low power constraint and designing novel communication schemes are of essential importance. In this work, we touch some aspects of this promising research area.

1.1 Problem Motivation

A point-to-point communication system is composed of a transmitter, a receiver and a channel. The transmitter sends a signal $\mathbf{x}$ to the receiver. The receiver receives a corrupted version $\mathbf{y}$ of the transmitted signal. One source of the channel corruption is the noise. Among various channel noise models, the Additive White Gaussian Noise (AWGN) model is probably the most widely used one. In AWGN channel model, the received signal is the sum of the transmitted signal and a Gaussian-distributed noise signal $\mathbf{w}$. It is known that the AWGN channel's capacity is $\frac{1}{2}\log\left(1+\frac{P}{N_0}\right)$ per degree of freedom, where P is the average input power constraint and N_0 is the variance of

the additive noise.

When transmitted in wireless channels, the signal is corrupted by not only additive noise but also multipath fading (explained in Chapter 2). However, most wireless channels can be reduced to narrowband flat fading channels, where the received signal is corrupted by time-varying multiplicative coefficients $\mathbf{h}$, called the fading coefficients. The exact value of fading coefficient is named Channel State Information (CSI). If CSI is available at both the transmitter and the receiver, then the fading channel capacity is achieved when the transmitter adapts its power, data rate and coding scheme to the CSI, e.g. "water-filling" over the time. In [1], the authors showed that, in some special cases, the availability of CSI at the receiver affects the decoding complexity but not the channel capacity. In [2], the authors proved that, in the wideband limit and under the average power constraint, the same capacity as the AWGN channel can be achieved, without CSI at either the transmitter or the receiver. The communication scheme to achieve the AWGN capacity, as proposed in [2] for the general multipath fading channel, is called "peaky signaling", which transmits at a low duty cycle and uses Frequency Shift Keying (FSK). Although "peaky signaling" can achieve the channel capacity in very severe conditions (no transmitter CSI or receiver CSI), there are many occasions where "peaky signaling" may not be a suitable choice. Possible concerns include physical device limitations, power supply and safety issues. For these scenarios, peak power constrained communication schemes may be a better choice than average power constrained communication schemes. In this thesis, we employ an input power constraint in between the above two type of constraints, which does not allow power reservation between different coherence blocks (to be defined in Chapter 2) but allows any power allocation scheme within a fading block.

Apart from different capacity-achieving communication schemes, wideband channel capacity under the average power constraint is also significantly different between the full transmitter CSI scenario and the no transmitter CSI scenario. On the one hand, the capacity formula in [1] for the full transmitter CSI scenario indicates that the channel capacity increases unboundedly as the bandwidth increases. On the other hand, in [2], the authors showed that the wideband capacity is $\frac{P}{N_0}$, for the scenario

without transmitter CSI. Therefore, the availability of the transmitter CSI has a great impact on the wideband capacity under the average power constraint.

CSI surely comes at a cost, since, although the statistical distribution of fading coefficients is available in most cases, the exact values of the fading coefficients are usually unknown and need to be estimated. The common method to obtain CSI at the receiver is through channel testing. The transmitter's CSI can then be obtained from the receiver if an error-free instantaneous feedback channel is available. Clearly, a portion of the transmitter's energy needs to be spent in sending channel testing sequences. The energy cost of channel testing is negligible in the high SNR (defined in Chapter 2; for now, just think of it as proportional to the input power) region. However, the channel testing cost for wideband channels can not be ignored in the low SNR region, since the energy per degree of freedom is so small that it is not sufficient to measure the channel accurately. In this scenario, we are usually only able to obtain some partial CSI with certain amount of channel testing cost.

To achieve higher data rates, we need to balance the energy consumption between channel testing and data transmission. Though not the optimal signaling scheme, BPSK signaling is enough to characterize the channel performance, under some special assumptions (explained in Chapter 2). Moreover, BPSK signaling greatly simplifies our analysis and allows us to focus on the main tradeoff which is between allotting more energy in channel testing and spending more energy in transmitting information. Thus, we convert the wideband channel to independent subchannels and model them as a set of independent Binary Symmetric Channels (BSC) through BPSK signaling. The subchannel quality is characterized as the BSC's crossover probability. Specifically, we are able to characterize the number of subchannels that should be probed for capacity maximization in terms of the available transmission energy, the available bandwidth and the fading characteristics. Although we are only able to derive analytical expressions for an upper bound and a lower bound on the desirable number of probed subchannels, the two bounds are so close to each other that they may well be treated as "approximation" rather than "bounds" to the desirable number of probed subchannels.

1.2 Thesis Outline

In Chapter 2, we explain in more details the setup of our communication model and the general structure of our communication scheme. In Chapter 3, a multi-armed bandit approach is carried out to study various channel testing algorithms. Finally, in Chapter 4, we design our communication scheme by specifying several parameters and present our main results.

Chapter 2

Wideband Fading Channel and Communication Schemes

Some special properties of wireless channels include the multipath property and the fading phenomena. In this chapter, we refer to the classical wireless channel model and formulate the particular problem to investigate in this thesis.

2.1 Multipath Fading Model

In wireless channels, there is usually more than one path from the transmitter to the receiver, with different path strengths and path lengths, which is referred to as the multipath property. One direct result of this property is that more than one copy of the transmitted signal arrives at the receiver through different paths, with different scalings and delays. In [3], the authors expressed the Input/Output (I/O) relation between the transmitted signal $x(t)$ and the received signal $y(t)$ in the following formula,

$$y(t) = \sum_i a_i(t)\, x(t - \tau_i(t)) + w(t)\,, \tag{2.1}$$

where the summation is taken over all significant paths. In (2.1), $a_i(t)$ and $\tau_i(t)$ are. respectively. the path gain and path delay of the i^{th} path at time t: $w(t)$ is the Additive Noise. which is usually assumed to be Additive White Gaussian Noise (AWGN). The

I/O relation (2.1) can be represented as a linear time-varying system,

$$y(t) = \int_{-\infty}^{+\infty} h(\tau, t)\, x(t-\tau)\, d\tau + w(t)\,, \tag{2.2}$$

$$\text{where} \quad h(\tau, t) = \sum_i a_i(t)\, \delta(\tau - \tau_i(t))\,. \tag{2.3}$$

where $h(\tau, t)$ in (2.3) is the impulse response of the I/O system at time t. By taking the Fourier Transform of (2.3), we have the following time-varying frequency response

$$H(f, t) = \int_{-\infty}^{+\infty} h(\tau, t)\, e^{-j2\pi f\tau}\, d\tau = \sum_i a_i(t)\, e^{-j2\pi f \tau_i(t)}\,. \tag{2.4}$$

In practice, communication is usually carried out over a frequency band W around the carrier frequency f_c, whose I/O relation is represented in (2.2). For convenience of analysis, the passband signals are down-converted to the baseband and sampled at the Nyquist sampling rate, W. Accordingly, the continuous I/O relation (2.2) reduces to the following discrete-time I/O formula,

$$y(m) = \sum_l h_l(m)\, x(m-l) + w(m)\,, \tag{2.5}$$

$$\text{where} \quad h_l(m) = \sum_i a_i^b\left(\frac{m}{W}\right) \text{sinc}[\, l - \tau_i\left(\frac{m}{W}\right) W\,]\,, \tag{2.6}$$

$$a_i^b(t) = a_i(t) e^{-j2\pi f_c \tau_i(t)}\,.$$

$x(m)$ and $y(m)$ denote the baseband input and output signal sampled at time $\frac{m}{W}$. $\{h_l(m)\}$ are the fading coefficients sampled at time $\frac{m}{W}$. The baseband AWGN sample sequence $\{w(m)\}$ forms a sequence of independent and identically distributed (i.i.d.) Gaussian random variables. Expression (2.5) actually represents a time-varying discrete-time filter, where $h_l(m)$ represents the l^{th} filter tap at time $\frac{m}{W}$.

The coherence time T_c (in the unit of seconds) of a wireless channel is the interval during which the channel does not vary significantly. In terms of the discrete-time model (2.5), the coherence time L_c (in the unit of samples) is the interval during which $h_l(m)$ does not change significantly as a function of m. T_c and L_c are related

by

$$T_c = L_c \frac{1}{W}. \tag{2.7}$$

The coherence bandwidth W_c is the width of the spectrum over which the channel frequency response $H(f,t)$ in (2.4) does not change significantly as a function of f. The delay spread T_d and the Doppler spread D_s are inversely proportional to the coherence bandwidth W_c and the coherence time T_c, respectively.

Fading channels are divided into two categories, depending on the relative amplitude between the coherence time T_C and the sampling interval $\frac{1}{W}$. If $\frac{1}{W} \ll T_c$, the fading channel is called a slow fading channel; If $\frac{1}{W} \gg T_c$, the fading channel is called a fast fading channel. The relative amplitude between the coherence time T_c and the sampling interval $\frac{1}{W}$ is closely related to the relative amplitude between the channel bandwidth W and the Doppler spread D_s. If $W \gg D_s$, then $\frac{1}{W} \ll T_c$; if $W \ll D_s$, then $\frac{1}{W} \gg T_c$. In most cases, the channel bandwidth W is much larger than the Doppler spread D_s. Therefore, we are mostly interested in the slow fading channels. Moreover, we use the following block fading channel model as a simplification for the slow fading channel: the time axis is segmented into consecutive disjoint coherence blocks, each of length T_c (seconds) or L_c (samples); the fading coefficient $\mathbf{h}_l(m)$ remains constant within each coherence block; the fading coefficients in different coherence blocks are mutually independent. We illustrate the block fading model in Figure 2-1, where the time axis is in the units of samples.

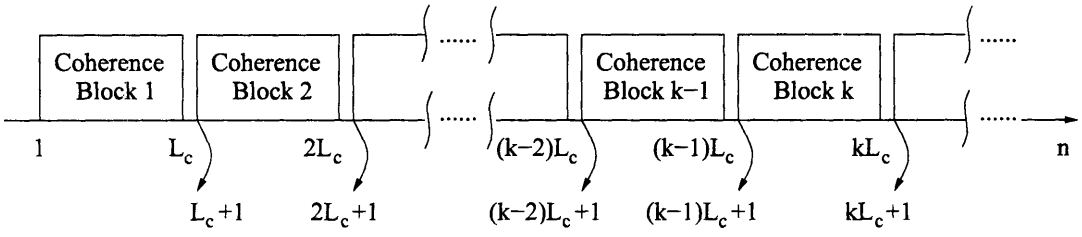

Figure 2-1: Block Fading Model in Discrete Time Scale

2.2 Narrowband Channel

In practice, the communication is usually carried out over a channel which occupies a band with finite width W (Hz). Such channels are divided into two categories, depending on the relative amplitude between the channel bandwidth W and the coherence bandwidth W_c. A channel is called narrowband if its bandwidth W is much smaller than the coherence bandwidth W_c; otherwise, it is called wideband. Recalling the definition of the coherence bandwidth W_c, a narrowband channel's frequency response is almost flat within its frequency band. Owing to the relation between the delay spread T_d and the coherence bandwidth, we have that for a narrowband channel,

$$T_d = \frac{1}{W_c} \ll \frac{1}{W} . \tag{2.8}$$

Therefore, if an impulse is transmitted, the significant part of the received signal spreads much smaller than the sampling interval $\frac{1}{W}$. Recall that, in the multi-tap discrete-time filter model (2.6), a filter tap contains all the paths whose delays are approximately within one sampling interval $\frac{1}{W}$. Since the delay spread of a narrowband channel T_d is much smaller than the sampling interval $\frac{1}{W}$ according to (2.8), one filter tap in the multi-tap discrete-time filter model (2.6) is sufficient to represent all significant paths in a narrowband channel. By suitably adjusting the time origin of the receiver, we can make this filter tap the 0^{th} tap in (2.6). Therefore, for a narrowband channel, the multi-tap discrete-time filter model (2.5 and 2.6) reduces to the following single-tap discrete time filter model

$$y(m) = h(m)\, x(m) + w(m) , \tag{2.9}$$

$$\text{where} \quad h(m) = \sum_i a_i^b \left(\frac{m}{W}\right) \text{sinc}[\, \tau_i \left(\frac{m}{W}\right) W\,] , \tag{2.10}$$

$$a_i^b(t) = a_i(t) e^{-j2\pi f_c \tau_i(t)} .$$

2.3 Wideband Channel

The bandwidth of a wideband channel W is usually much larger than the coherence bandwidth W_c. Therefore, the previous narrowband channel model is no longer suitable. In particular, it is no longer suitable to assume that the frequency response of the wideband channel is still flat within its bandwidth. Moreover, if the Nyquist Sampling rate $\frac{1}{W}$ is used for a wideband channel, the single-tap discrete-time filter model (2.9 and 2.10) no longer applies, since the delay spread usually extends over multiple sampling intervals.

To utilize the wideband channel, we convert it to multiple narrowband subchannels and then deal with each subchannel separately. We will not investigate various methods of converting a wideband channel into narrowband subchannels. Rather, we assume that the conversion is done in such a way that the resulting subchannels are narrowband and mutually independent. The L narrowband subchannels are centered at $\{f_l,\ l = 1, 2, \ldots, L\}$, where $L \gg 1$. The l^{th} subchannel occupies the frequency band from $f_l - \frac{W}{2}$ to $f_l + \frac{W}{2}$. Since the subchannels are narrowband, we can apply the single-tap discrete-time I/O model (2.9) and (2.10). Therefore, for the l^{th} subchannel,

$$y_l(m) \;=\; h_l(m)\, x_l(m) + w_l(m)\,, \tag{2.11}$$

where the sampling rate is assumed to be W. $h_l(m)$ is the fading coefficient of the l^{th} subchannel. $x_l(m)$ and $y_l(m)$ denote, respectively, the discrete-time baseband input and output to the l^{th} subchannel at time $\frac{m}{W}$.

2.4 Statistical Channel Model

Now, we have L narrowband subchannels, each represented by a single-tap discrete-time I/O relation (2.11), which describes the particular scenario where the input sequence $\{x_l(m).\, l = 1, \ldots, L.\, m \in \mathbb{N}\}$ is sent over the subchannels characterized by the fading coefficient sequence $\{h_l(m).\, l = 1, \ldots, L.\, m \in \mathbb{N}\}$ and the additive noise sequence $\{w_l(m).\, l = 1, \ldots, L.\, m \in \mathbb{N}\}$. However, a communication system is expected

to work not only in a particular scenario, but also in a family of scenarios with different parameters. Therefore, a statistical channel model is more suitable and helpful when designing the communication system. Hence, we treat the fading coefficients as random variables and assign to them particular probability distributions. Thus, the single-tap discrete-time I/O relation (2.11) is modified to the following statistical channel model,

$$\mathbf{y}_l(m) = \mathbf{h}_l(m)\,\mathbf{x}_l(m) + \mathbf{w}_l(m)\,, \tag{2.12}$$

where we use bold face for random variables. The AWGN noise sequence $w_l(m)$ is assumed to be i.i.d. Circularly Symmetric Gaussian random variables with variance N_0. The distribution of the fading coefficients will be specified in later sections.

As described in the previous section, each subchannel's bandwidth W is smaller than the coherence bandwidth W_c (flat fading) and W is greater than the Doppler spread D_s (slow fading). Furthermore, the block fading assumption is adapted as follows for the statistical channel model: *At the beginning of each coherence block, the subchannel's fading coefficient* $\boldsymbol{h}$ *takes a realization according to a particular distribution* $f_{\mathbf{h}}(h)$*, independently of the fading coefficients in the previous and following coherence blocks; the* L *subchannels select fading coefficients mutually independently according to the same distribution* $f_{\mathbf{h}}(h)$*; the fading coefficients remain constant within each coherence block.*

Signal-to-Noise-Ratio (SNR) denotes the ratio of the average received signal power to the average received noise power.

$$\mathsf{SNR} = \frac{\mathcal{E}\left[\left|\sum_l \sum_m \mathbf{h}_l(m)\,\mathbf{x}_l(m)\right|^2\right]}{\mathcal{E}\left[\left|\sum_l \sum_m \mathbf{w}_l(m)\right|^2\right]}$$

$$= \mathcal{E}\left[|\mathbf{h}|^2\right] \frac{\mathcal{E}\left[\sum_l \sum_m |\mathbf{x}_l(m)|^2\right]}{\mathcal{E}\left[\sum_l \sum_m |\mathbf{w}_l(m)|^2\right]} \tag{2.13}$$

$$= \mathcal{E}\left[|\mathbf{h}|^2\right] \frac{P}{N_0 B}. \tag{2.14}$$

where B is the bandwidth of the wideband channel. Step (2.13) follows from the assumption that the fading coefficients are i.i.d. random variables with the same distribution and they are independent of the input sequence and the noise sequence.

Remark 1 P is the average power constraint on the input sequence, which is expressed as follows.

$$\lim_{m_0 \to \infty} \sup \frac{\sum_l \sum_{m=1}^{m_0} |\mathbf{x}_l(m)|^2}{\frac{1}{W} m_0} \leq P, \tag{2.15}$$

where $\frac{1}{W} m_0$ is the time in seconds for a length-m_0 input sequence.

Remark 2 If the average input power P is fixed in (2.14), then the Signal-to-Noise-Ratio SNR decreases as the bandwidth B increases. This is due to the fact that more noise power is collected by the receiver as the bandwidth increases while the input power remains constant, resulting in a decreasing SNR.

The actual value of the fading coefficients $\{\mathbf{h}_l(m)\}$ is called the Channel State Information (CSI). For fast fading channels, it is useless to estimate the channel states, since the channel states vary from time to time. However, for block fading channels, the channel states remain constant within each coherence block, which usually spreads over hundreds to thousands of samples. Therefore, it is possible to estimate the channel states in block fading channels. The common method in practice to estimate the channel states is that the transmitter sends a training sequence in each coherence block, the receiver compares the received sequence with the transmitted sequence and then estimates the channel states. With the help of a noiseless feedback channel, the transmitter synchronizes with the receiver and gains the same

knowledge of the channel states. This method works well on a single narrowband channel, but it is not clear how the training-based communication scheme should be generalized to a large number of narrowband subchannels. The underlying difficulty is that the number of subchannels is large ($L \gg 1$) but the average input power is constrained. Estimating channel states of more subchannels requires more power allocated into training sequences, necessarily reducing the power available for transmitting information-bearing sequences. We shall focus on this tradeoff between channel testing and data transmission. Before the analysis on the above tradeoff unfolds, we first make several assumptions to clarify further our problem setup.

2.5 Modulation and Demodulation

For our investigation, BPSK is employed as the modulation scheme, both for the channel testing phase and for the data transmission phase. The BPSK constellation is composed of two signal points, $+1$ and -1. We assume that the same BPSK constellation $\{+1, -1\}$ is used for all subchannels. On each subchannel, the BPSK constellation remains the same over the time. Each BPSK symbol consumes one unit energy, due to the $\{+1, -1\}$ constellation. If we use E_k to denote the number of BPSK symbols sent in the k^{th} coherence block on all subchannels, then the average power constraint on the input sequence (2.15) reduces to

$$\lim_{k_0 \to \infty} \sup \frac{\sum_{k=1}^{k_0} E_k}{k_0} \leq P T_c, \tag{2.16}$$

which means that the average energy consumption of the input sequence per block is at most PT_c. If (2.16) is the only power constraint on the input sequence, then the transmitter is allowed to reserve energy for future use. As we have mentioned in the introduction, stricter input power constraint may be of interest to tackle the concerns like physical device limitations, power supply and safety issues. Therefore, we do not allow power reservation between different coherence blocks but allow any

power allocation within a fading block. The average energy constraint (2.16) reduces to the following per block energy constraint,

$$E_k \leq P T_c\,, \quad \text{for } \forall\, k\,. \tag{2.17}$$

The input to the l^{th} subchannel, $\{\mathbf{x}_l[m]\}$, is a binary sequence composed of symbol 0 and symbol 1. The modulator maps each symbol $\mathbf{x}_l[m]$ ($\mathbf{x}_l[m] \in \{0,1\}$) to a signal point $\mathbf{x}_l(m)$ ($\mathbf{x}_l(m) \in \{+1,-1\}$) in the following way,

$\mathbf{x}_l[m]$	$\mathbf{x}_l(m)$
0	+1
1	−1

We use $\mathbf{y}_l(m), \mathbf{h}_l(m), \mathbf{w}_l(m)$ to denote the sample value of the received signal process, fading coefficient process and the additive noise process at time $\frac{m}{W}$, respectively.

Since the input sequence is modulated symbol by symbol, there is no loss of performance if the demodulator at the receiver makes decision on each received $\mathbf{y}_l(m)$ separately. Owing to the I/O relation (2.11) and the AWGN assumption, the optimal demodulator is illustrated in Figure 2-2. Assuming that all other components in the

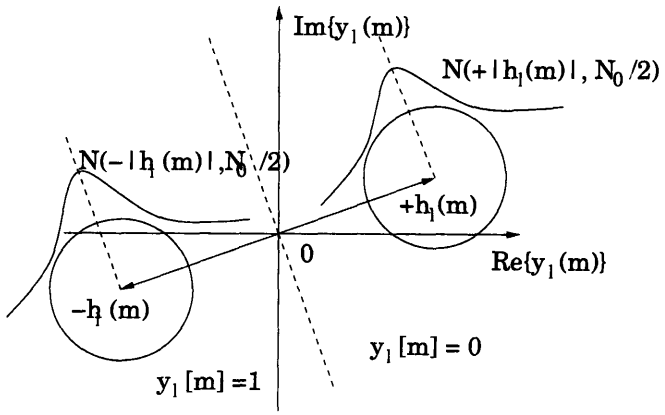

Figure 2-2: Demodulate the Received Signal: $\mathbf{y}_l(m)$ to $\mathbf{y}_l[m]$

communication system are error-free except for the demodulator. the error probability

of each input binary symbol to the l^{th} subchannel is,

$$\mathbf{P}(\mathbf{y}_l[m] = 1 \,|\, \mathbf{x}_l[m] = 0) = Q\left(\frac{|\mathbf{h}_l(m)|}{\sqrt{\frac{N_0}{2}}}\right), \tag{2.18}$$

$$\mathbf{P}(\mathbf{y}_l[m] = 0 \,|\, \mathbf{x}_l[m] = 1) = Q\left(\frac{|\mathbf{h}_l(m)|}{\sqrt{\frac{N_0}{2}}}\right), \tag{2.19}$$

$$\mathbf{P}_l = \mathbf{P}(\mathbf{y}_l[m] = 1 \,|\, \mathbf{x}_l[m] = 0) = \mathbf{P}(\mathbf{y}_l[m] = 0 \,|\, \mathbf{x}_l[m] = 1). \tag{2.20}$$

Therefore, the l^{th} subchannel can be represented as a Binary Symmetric Channel (BSC), with crossover probability $\mathbf{P}_l$.

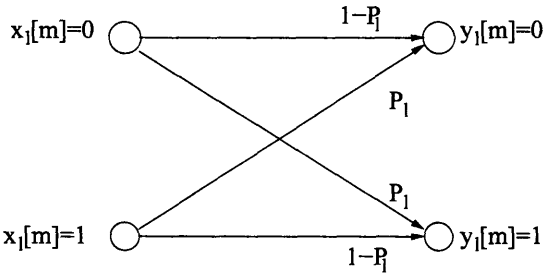

Figure 2-3: The BSC Representation for the l^{th} Subchannel

Incorporating the noiseless feedback channel within the channel testing phase, the system diagram of the l^{th} subchannel is illustrated in Figure 2-4.

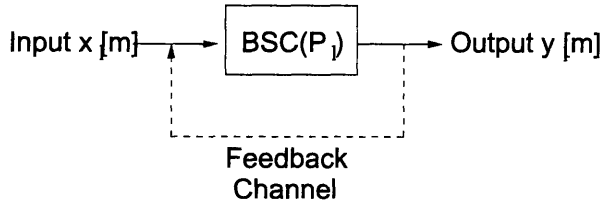

Figure 2-4: System Diagram for the l^{th} Subchannel

The crossover probability $\mathbf{P}_l$ characterizes the l^{th} subchannel's quality. The noiseless feedback channel is represented as a dotted line in Figure 2-4 to emphasize that it only duplicates the testing results to the transmitter. After the testing phase, the feedback channel is not used. Each subchannel is used as an ordinary BSC

without feedback during the transmission phase. Thus, we are investigating the impact of the transmitter CSI on the achievable rate rather than studying the feedback communication.

2.6 Two-Level Fading Model

The expression for the l^{th} subchannel crossover probability in (2.20) indicates that, with coherent detection, $\mathbf{P}_l$ is only related to the fading coefficient amplitude $|\mathbf{h}_l(m)|$. Although the Raleigh or Nakagami distribution are commonly used for fading coefficient amplitude, their expressions are pretty complicated, which makes our further analysis much harder. Instead, we consider the two-level fading model, which is much simpler to analyze but still captures most of the aspects we are concerned with. In the two-level fading model, the amplitude of each fading coefficient can be either h_G or h_B. The probability distribution of $\mathbf{h}$ reduces to the following Probability Mass Function (PMF) of $|\mathbf{h}|$.

$$\mathbf{P}[\,|\mathbf{h}| = h_B\,] = \sigma \tag{2.21}$$

$$\mathbf{P}[\,|\mathbf{h}| = h_G\,] = 1-\sigma\,. \tag{2.22}$$

where $h_B > h_G \geq 0$.

The two-level fading model asserts that the subchannels must be in one of two possible states. The "good" state is associated with the larger fading coefficient amplitude h_G and the "bad" state is associated with the smaller amplitude h_B. Each subchannel chooses between the two states at the beginning of each coherence block according to the PMF in (2.21, 2.22) and keeps that state in the block.

2.7 Communication Scheme

In our communication scheme, each coherence block is composed of two parts, channel testing phase and data transmission phase, as illustrated in Figure 2-5.

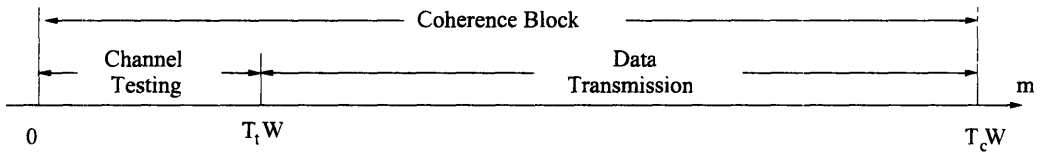

Figure 2-5: Coherence Block Structure: Channel Testing Phase and Data Transmission Phase

Before communication starts, the transmitter and the receiver agree on what channel testing sequence to send for each coherence block and how they should be sent. During each coherence block, the pre-configured training sequences are sent in the pre-configured way. The receiver demodulates the noise-corrupted received sequence, compares them with the pre-configured channel testing sequences and updates its estimates of the CSI. The receiver's CSI estimates are then immediately feedback to the transmitter through the noiseless feedback channel. As explained in previous sections, the noiseless feedback channel only duplicates the receiver's testing results to the transmitter; after the testing phase, the feedback channel is not used; each subchannel is used as an ordinary BSC without feedback during the transmission phase. This assumption may be suitable for the scenario where feedback channel resource is rare, expensive and should be used less.

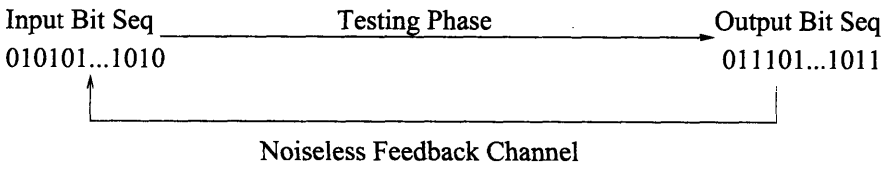

Figure 2-6: Channel Testing Phase with Noiseless Feedback Channel

When the channel testing ends, the transmitter allots the remaining energy onto the chosen subchannels for data transmission, according to the estimated CSI. We use E_{te}, E_{tr} $(E_{te} + E_{tr} = PT_c)$ to denote the energy for channel testing and data transmission.

Recall that in (2.14), the relation between the wideband channel bandwidth B, the input power constraint P and the received Signal-Noise-Ratio SNR was provided. Given that N_0 and $\mathbb{E}[|\mathbf{h}|^2]$ are fixed, the SNR per degree of freedom decreases as

the channel bandwidth B increases. This means that for a wideband channel with a very large bandwidth B, the SNR is not large enough to accurately estimate the channel states. We make this observation explicit by requiring that each input symbol should consume a constant amount of energy (one unit for our BPSK constellation). Therefore, the energy allocated into the channel testing phase (respectively, the data transmission phase) is equivalent to the number of BPSK symbols sent during each phase, respectively.

On the other hand, BPSK may not be the most suitable signaling scheme for the transmission phase. However, we characterize the subchannel only by its achievable rate. The rates of different signaling schemes all increase as the fading coefficient amplitude $|\mathbf{h}_l(m)|$ increases. Since this relation between rate and $|\mathbf{h}_l(m)|$ is enough for our investigation of the tradeoff between channel testing and data transmission, BPSK is as good as other more complicated signaling scheme. Thus, fixed-level BPSK is also used for modulating the information-bearing sequences during the transmission phase.

Our communication scheme structure is as follows.

Communication Scheme Structure

1. We segment the time axis into coherence blocks, each of length T_c (Figure 2-1): We also convert the wideband channel into a large number of narrowband subchannels, each of bandwidth W.

2. During each coherence block, the transmitter repeats the following steps.

   Step 1 When the coherence block starts, the transmitter takes M subchannels at random. The transmitter spends E_{te} units of energy in testing these M subchannels with a pre-configured Median Deletion Algorithm (MDA). When MDA terminates, it returns the selected subchannel, denoted as subchannel I.

   Step 2 The transmitter then spends the remaining energy in transferring data over the selected subchannel I.

Remark 1 In the communication scheme, we implicitly assume that only one subchannel is chosen for transmission. We use the following figure to explain this assumption. In Figure 2-7, subchannel 1 is the best and subchannel 2 is the second best according to the testing results. In the upper Figure 2-7, where T_c is small, not all the E_{tr} energy can be consumed by the end of T_c if the transmission is only carried out over subchannel 1. Under this condition, we should also choose subchannel 2. In the lower Figure 2-7, where T_c is large, we are able to use all the E_{tr} energy by the end of T_c on subchannel 1. Since the 1st subchannel has a better quality than any other subchannel according to the testing results, it is desirable to transmit over subchannel 1 only. For a fixed amount of energy E per coherence block, the input power is inversely proportional to the coherence time T_c. Since we are mostly interested in the very low SNR scenario, it is reasonable to assume that T_c is large enough compared with E such that, within each coherence block, the transmission energy E_{tr} can be consumed on one subchannel by the end of the coherence block. This relation between T_c and E guarantees no loss of performance if we only choose the

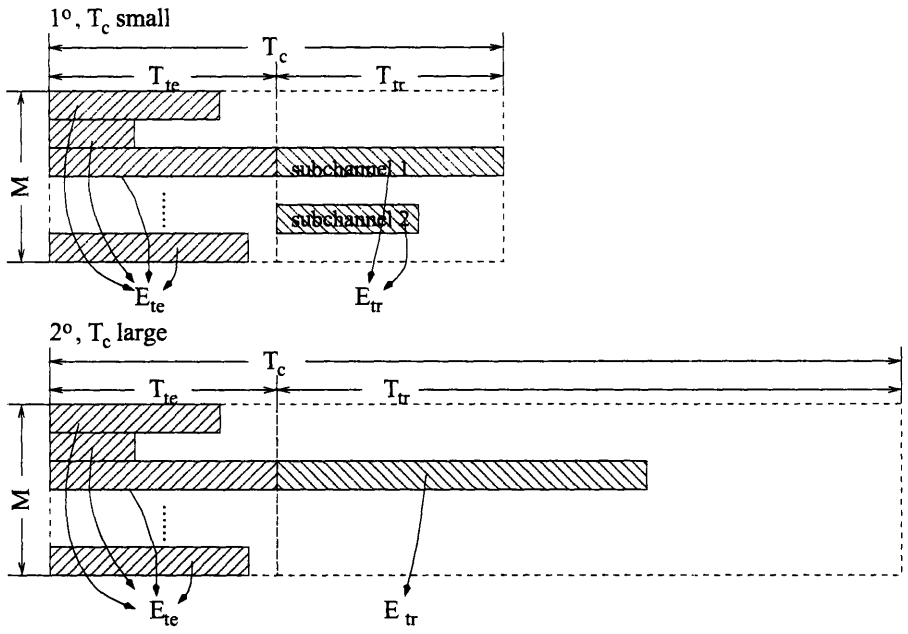

Figure 2-7: Examples: How T_c affects Channel Selection

best subchannel for transmission.

2.8 Summary

In this section, we have introduced the wideband fading channel and our scheme to communicate on it. We focus on the very low SNR communication scenario where the Channel State Information is not a-priori available at the transmitter. To deal with the lack of transmitter CSI, training and feedback channel are utilized. BPSK modulation and coherent detection are also assumed, so that the tradeoff between channel testing and data transmission can be characterized with relative ease.

At the current step, we have two problems to solve. The first is what algorithm we should use for channel testing. The second is how big a portion of the wideband channel we should test, or equivalently, how many subchannels we should test. The first problem is important, since otherwise our communication scheme is incomplete. We shall deal with this problem in Chapter 3. The second problem is equivalent to the tradeoff between channel testing and data transmission. We shall come back to

this problem in Chapter 4.

Chapter 3

Multi-Armed Bandit Problem and Channel Testing Algorithm

In Chapter 2, we described the general structure of our communication scheme. In this chapter, we focus on the testing phase of each coherence block. Here, we list the communication scheme per coherence block, as described in Chapter 2.

Communication Scheme Structure

Step 1 When the coherence block starts, the transmitter takes M subchannels at random. The transmitter spends E_{te} units of energy in testing these M subchannels with a pre-configured channel testing algorithm. When the channel testing algorithm terminates, it returns the selected subchannel, denoted as subchannel I.

Step 2 The transmitter then spends the remaining energy in transferring data over the selected subchannel I.

Under BPSK modulation with fixed constellation $\{+1, -1\}$, each subchannel is represented as a BSC with quality being characterized by its crossover probability $\mathbf{P}$. Before testing, all the subchannels have the same a-priori quality distribution $f_{\mathbf{P}}(p)$. Therefore, in "Step 1", we randomly select M subchannels without any preference.

When the coherence block starts, the crossover probabilities $\{ \mathbf{P}_l, l = 1, \ldots, M \}$ take independent realizations according to $f_{\mathbf{P}}(p)$, which is unknown to the transmitter. Without loss of generality, the domain of $f_{\mathbf{P}}(p)$ is assumed to be $[0, \frac{1}{2}]$. Clearly, within this range, subchannels with smaller crossover probabilities have better qualities. Since the crossover probabilities $\{ \mathbf{P}_l, l = 1, \ldots, M \}$ keep constant within the coherence block, it is possible for the transmitter to find the best-quality subchannel through testing. Since each BPSK symbol consumes 1 unit of energy, the E_{te} units of testing energy allows us to input E_{te} testing symbols into the M subchannels. Thus, the transmitter uses the M subchannels for a total of E_{te} times in any sequence, and makes a decision on which subchannel to use for transmission.

The above setup of searching for the best-quality subchannel is similar to the Multi-Armed Bandit Problem (MABP), originally described in [4]. An algorithm designed to solve the MABP can be adapted to a channel testing algorithm with minor modification. Therefore, in this chapter, we study the MABP and its algorithms.

3.1 Multi-Armed Bandit Problem

As described in [4], the MABP's problem setup is as follows.

A gambler is provided with M slot machines, denoted as machine $1, \ldots, M$. The reward of each slot machine forms a stochastic process, called the reward process: if the i^{th} machine is tried at time t, a random reward $\boldsymbol{R}_i(t)$ is received. The sequence of random rewards $\{\boldsymbol{R}_i(t), t = 1, 2, \ldots\}$ are independent identically distributed (i.i.d). The reward processes of the M slot machines are mutually independent. The gambler's objective is to maximize the total received rewards by designing a strategy specifying which slot machine to try at each time step.

Despite its simplicity, the MABP encompasses the important tradeoff between exploration and exploitation. On the one hand, the gambler should explore more slot machines, with the hope of finding a machine better than those tried. On the other hand, the gambler should rather exploit a slot machine that he thinks is good and keep on using it to collect rewards. There are drawbacks in either direction. First

of all, if the gambler spends too much time exploring different machines, he may possibly not be able to try the good ones enough to collect rewards. Secondly, if the gambler keeps on exploiting the machine which he believes to be good, he may miss other better machines.

MABP is a classical problem in the control and decision making area, and has been studied in various setups. In [5], the authors have made a comprehensive survey of the classical results related to MABP. However, these classical approaches are not suitable for our problem setup. The transmitter is not sending informational bits but testing symbols during the testing phase. Furthermore, the transmitter can send at most E_{te} testing symbols during the testing phase. This problem setup corresponds to a special MABP where the gambler's objective is not to maximize the received rewards but to collect information about machine qualities. Clearly, within a finite number of machine tests, it is not possible for the gambler to find the best slot machine with 100% confidence. To achieve a precise estimate of even one machine's quality, an infinite number of tests are required.

The Probably Approximately Correct (PAC) approach to MABP, recently proposed by Even-Dar et al in [8], is a suitable way to deal with our problem setup. In PAC MABP, the gambler's objective is not to collect rewards but to find a near-optimal slot machine with high confidence. This agrees with the implicit assumption in our problem setup that the transmitter nails down his selection on one slot machine when testing ends. We assume that each random reward $\mathbf{R}_i(t)$ is a binary random variable taking value in $\{0, 1\}$.

$$\mathcal{P}[\mathbf{R}_i(t) = 1] = p_i, \tag{3.1}$$

$$\mathcal{P}[\mathbf{R}_i(t) = 0] = 1 - _i . \tag{3.2}$$

We don't use the bold face for p_i since, in our communication scenario, the channel testing is done within one coherence block, where the subchannel's state remains unchanged. $\{p_i, i = 1, \ldots, M\}$ are unknown to the gambler. Let r_i denote the average

reward of the i^{th} slot machine, we have that

$$r_i \;=\; \mathcal{E}[\,\mathbf{R}_i\,]\,. \tag{3.3}$$

Let $I_\star$ denote the index of the optimal slot machine, then

$$\mathcal{E}[\,\mathbf{R}_{I_\star}\,] = \max_{i=1,\ldots,M} \mathcal{E}[\,\mathbf{R}_i\,]\,, \tag{3.4}$$

$$I_\star = \arg\max_{i=1,\ldots,M} \mathcal{E}[\,\mathbf{R}_i\,]\,. \tag{3.5}$$

Furthermore, the ϵ-optimal slot machine is defined as follows: a machine is ϵ-optimal if its average reward is greater than $\mathcal{E}[\,\mathbf{R}_{I_\star}\,] - \epsilon$.

$$\mathcal{E}[\,\mathbf{R}_k\,] > \mathcal{E}[\,\mathbf{R}_{I_\star}\,] - \epsilon \;\;\rightarrow\;\; \text{machine } k \text{ is } \epsilon\text{-optimal}\,, \tag{3.6}$$

$$\mathcal{E}[\,\mathbf{R}_k\,] \leq \mathcal{E}[\,\mathbf{R}_{I_\star}\,] - \epsilon \;\;\rightarrow\;\; \text{machine } k \text{ is not } \epsilon\text{-optimal}\,. \tag{3.7}$$

Clearly, the optimal machines themselves are also ϵ-optimal. In PAC MABP, the gambler's objective is to design a testing algorithm which outputs an ϵ-optimal slot machine with probability at least $1 - \delta$. We call any algorithm that achieves this performance an (ϵ, δ)-PAC algorithm. Let I denote the index of the selected machine, then the above (ϵ, δ)-PAC performance can be expressed as follows,

$$\mathcal{P}\{\mathcal{E}[\,\mathbf{R}_I\,] > \mathcal{E}[\,\mathbf{R}_{I_\star}\,] - \epsilon\} > 1 - \delta\,. \tag{3.8}$$

We assume that the randomness in (3.8) comes from the random rewards only. This essentially means that we don't consider any random algorithm.

It is not hard to see that the (ϵ, δ)-PAC performance is achievable with a finite number of trials. Furthermore, various algorithms achieve the (ϵ, δ)-PAC performance. Therefore, we need to compare these (ϵ, δ)-PAC algorithms using other metrics. Let $\mathbf{T}$ denote the number of machine trials for the algorithm to terminate. Then we define the complexity of a testing algorithm to be $\mathcal{E}[\,\mathbf{T}\,]$, the average number of machine trials. We compare various (ϵ, δ)-PAC algorithms by their complexities. The

gambler's objective is to design an (ϵ, δ)-PAC testing algorithm which has the minimal complexity. The positive parameter δ characterizes the gambler's confidence of his choice and the positive parameter ϵ specifies the quality of the gambler's selection.

3.2 Testing Algorithms

3.2.1 General Structure

In this section, we give a description for the general structure of the testing algorithms we consider.

Clearly, in a machine testing algorithm, we need to record the reward history of the tested machines. Owing to our binary reward assumption, the sufficient statistic for the average reward r_i of the i^{th} machine, given the reward history $\mathbf{R}_i(1), \ldots, \mathbf{R}_i(t)$ up to time t, is

$$\hat{\mathbf{P}}_i(t) = \frac{\mathbf{R}_i(1) + \cdots + \mathbf{R}_i(t)}{t}. \tag{3.9}$$

Therefore, we only need to keep a record of $\{\hat{\mathbf{P}}_i(t)\}$ as the algorithm proceeds. At each time step t, we keep an up-to-date average reward vector $\left(\hat{\mathbf{P}}_1(t), \ldots, \hat{\mathbf{P}}_M(t)\right)$. Based on this updated average reward vector, we make decisions on whether we should terminate, which machines to test at the next step and which machine to select if we decide to terminate. Here are two observations which affect the testing algorithm structure.

- The slot machines are mutually independent when they are tried simultaneously. Therefore, without loss of generality, we assume that, as the algorithm proceeds, we are allowed to try more than one machine in each time step.

- When the algorithm proceeds to time t, if we decide to stop trying the i^{th} machine due to its inferior performance, then we should not try it again at time t' later than t. If we stop trying the i^{th} machine at time t but resume trying it at time $t' > t$, then we could have made the trial on the i^{th} machine at time t

instead of time t', resulting in a better decision at time t and the same decision at time t'. The reason is that the testing results at time t' can not be used at time t, but the the testing results at time t can be used at time t'. Therefore, if we decide to stop trying the i^{th} machine at time t, then we say that the i^{th} machine is "deleted" at time t, indicating that it should not be tried again.

We use $\mathbf{T}$ to denote the time when the algorithm terminates, $\Omega(t)$ to denote the set of machines tested at time t and $M(t)$ to denote the size of the tested machine set at time t. We require our testing algorithm to satisfy,

$$\Omega(1) = \{1, \ldots, M\}, \tag{3.10}$$

$$\Omega(\mathbf{T}) = \{I\}, \tag{3.11}$$

$$\Omega(t) \supseteq \Omega(t+1) \qquad t = 1, \ldots, \mathbf{T}-1, \tag{3.12}$$

$$M(1) = M, \tag{3.13}$$

$$M(\mathbf{T}) = 1, \tag{3.14}$$

$$M(t) \geq M(t+1) \qquad t = 1, \ldots, \mathbf{T}-1. \tag{3.15}$$

Through (3.12), we require that, if a machine is not tried at time t, then it is excluded from the candidate sets $\Omega(t+1), \ldots, \Omega(\mathbf{T})$.

Here are some of the (ϵ, δ)-PAC algorithms, which satisfy the above structure.

3.2.2 Block Deletion Algorithm (BDA)

A very simple testing algorithm named block deletion algorithm (BDA) was described in [8]. In BDA, each machine is tested for the same number of times and the selection is made based on that testing history. To describe BDA in the previous general algorithm structure, the parameters $\Omega(t)$ and $M(t)$ are specified as follows,

$$\Omega(t) = \{1, \ldots, M\} \qquad t = 1, \ldots, \mathbf{T}, \tag{3.16}$$

$$M(t) = M \qquad t = 1, \ldots, \mathbf{T}. \tag{3.17}$$

Therefore. BDA makes decision at time $\mathbf{T}$ and outputs the machine with the greatest average reward.

$$I \;=\; \arg \max_{i=1,\ldots,M} \hat{\mathbf{P}}_i(\mathbf{T})\,. \tag{3.18}$$

The detailed structure of BDA is listed here.

Block Deletion Algorithm (ϵ, δ)

Step 1 Set $t = 1$ and the candidate machine set $S(t) = \{\,1, \ldots, M\,\}$.

Step 2 At time $t \in \{\,1, \ldots, M\,\}$, try every slot machine in $S(t)$ for once and update the average reward vector $\left(\hat{\mathbf{P}}_1(t), \ldots, \hat{\mathbf{P}}_M(t)\right)$. If $t < \mathbf{T}$, then set $S(t+1) = S(t)$, $t = t + 1$ and repeat **Step 2**; otherwise, continue to **Step 3**.

Step 3 Output the machine I who has the greatest average reward in $\left(\hat{\mathbf{P}}_1(\mathbf{T}), \ldots, \hat{\mathbf{P}}_M(\mathbf{T})\right)$.

Before proceeding to analyze BDA's performance, we first introduce the following Hoeffding Inequality (originally proposed and proved in [6]), which will be repeatedly used in this chapter.

Lemma 1. *(Hoeffding) Suppose $\boldsymbol{X}_1, \ldots, \boldsymbol{X}_n$ are independent random variables with finite first and second moments. Furthermore, assume that the $\boldsymbol{X}_i$ are bounded; that is, assume for $1 \leq i \leq n$ that*

$$\mathbb{P}(\boldsymbol{X}_i \in [a_i, b_i]) \;=\; 1 \tag{3.19}$$

(meaning that X_i is guaranteed to fall within the interval from a_i to b_i) then for the sum of these variables

$$\boldsymbol{S} \;=\; \boldsymbol{X}_1 + \cdots + \boldsymbol{X}_n\,, \tag{3.20}$$

we have the inequality

$$\mathcal{P}(\boldsymbol{S} - \mathcal{E}[\boldsymbol{S}] \geq n\epsilon) \leq \exp\left(-\frac{2n^2\epsilon^2}{\sum_{i=1}^{n}(b_i - a_i)^2}\right). \tag{3.21}$$

Remark 2: In the lemma, only one side of the inequality is provided, which can be easily extended. Suppose $\mathbf{Y}_1 = -\mathbf{X}_1, \ldots, \mathbf{Y}_n = -\mathbf{X}_n$, then $\mathbf{Y}_i, \ldots, \mathbf{Y}_n$ are independent, with finite first and second moments. $\mathbf{Y}_i$ is bounded within the interval $[-b_i, -a_i]$; that is, for $1 \leq i \leq n$ that $\mathcal{P}(\mathbf{Y}_i \in [-b_i, -a_i]) = 1$. Owing to Lemma 1, we have the following inequality for the sum $\mathbf{S}' = \mathbf{Y}_i + \cdots + \mathbf{Y}_n$:

$$\mathcal{P}(\mathbf{S}' - \mathcal{E}[\mathbf{S}'] \geq n\epsilon) \leq \exp\left(-\frac{2n^2\epsilon^2}{\sum_{i=1}^{n}((-a_i) - (-b_i))^2}\right). \tag{3.22}$$

Since $\mathbf{S}' = \mathbf{Y}_i + \cdots + \mathbf{Y}_n = -(\mathbf{X}_1 + \cdots + \mathbf{X}_n) = -\mathbf{S}$, we have that

$$\mathcal{P}(\mathbf{S} - \mathcal{E}[\mathbf{S}] \leq n\epsilon) \leq \exp\left(-\frac{2n^2\epsilon^2}{\sum_{i=1}^{n}(b_i - a_i)^2}\right), \tag{3.23}$$

which is the other side of the inequality as desired.

With the Hoeffding inequality in Lemma 1, we are ready to characterize BDA's testing length $\mathbf{T}$, which is summarized in the following lemma.

Lemma 2. *The Block Deletion Algorithm as listed above is (ϵ, δ)-PAC, if its testing length $\boldsymbol{T}$ is no less than $\frac{4}{\epsilon^2}\ln\frac{2(M-1)}{\delta}$,*

Proof. Suppose the k^{th} slot machine is not ϵ-optimal, at its average reward at time $\mathbf{T}$ is $\hat{\mathbf{P}}_k(\mathbf{T})$. Also, suppose machine $I_\star$ is one of the optimal machines. Let $r_\star = \mathcal{E}[\mathbf{R}_{I_\star}]$ and $r_k = \mathcal{E}[\mathbf{R}_k]$. Their relative locations are illustrated in the following figure.

Now, we estimate the rare event that the optimal machine performs worse than a

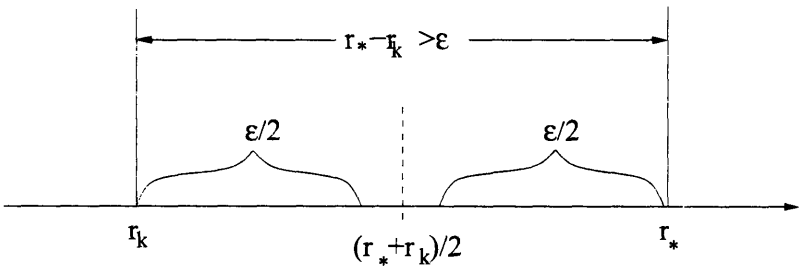

Figure 3-1: Locations of the Optimal Reward $r_\star$ and a Non-ϵ-Optimal Reward r_k

non-ϵ-optimal machine, i.e. $\hat{\mathbf{P}}_k(\mathbf{T}) > \hat{\mathbf{P}}_{I^*}(\mathbf{T})$.

$$
\begin{aligned}
& \mathcal{P}(\hat{\mathbf{P}}_k(\mathbf{T}) > \hat{\mathbf{P}}_{I_\star}(\mathbf{T})) \\
= \; & \mathcal{P}\left(\hat{\mathbf{P}}_k(\mathbf{T}) > \hat{\mathbf{P}}_{I_\star}(\mathbf{T}), \hat{\mathbf{P}}_{I_\star}(\mathbf{T}) < r_\star - \frac{\epsilon}{2}\right) \\
& + \mathcal{P}\left(\hat{\mathbf{P}}_k(\mathbf{T}) > \hat{\mathbf{P}}_{I_\star}(\mathbf{T}), \hat{\mathbf{P}}_{I_\star}(\mathbf{T}) \geq r_\star - \frac{\epsilon}{2}\right) && (3.24) \\
= \; & \mathcal{P}(\hat{\mathbf{P}}_k(\mathbf{T}) > \hat{\mathbf{P}}_{I_\star}(\mathbf{T}), \hat{\mathbf{P}}_{I_\star}(\mathbf{T}) < r_\star - \frac{\epsilon}{2}) \\
& + \mathcal{P}(\hat{\mathbf{P}}_k(\mathbf{T}) > \hat{\mathbf{P}}_{I_\star}(\mathbf{T}), \hat{\mathbf{P}}_{I_\star}(\mathbf{T}) \geq r_\star - \frac{\epsilon}{2}, \hat{\mathbf{P}}_k(\mathbf{T}) > r_k + \frac{\epsilon}{2}) && (3.25) \\
\leq \; & \mathcal{P}(\hat{\mathbf{P}}_{I_\star}(\mathbf{T}) < r_\star - \frac{\epsilon}{2}) + \mathcal{P}(\hat{\mathbf{P}}_k(\mathbf{T}) > r_k + \frac{\epsilon}{2}) && (3.26) \\
\leq \; & 2\exp\left(-(\frac{\epsilon}{2})^2\mathbf{T}\right). && (3.27)
\end{aligned}
$$

Remark 1 Equality (3.24) comes from the fact that

$$
\begin{aligned}
& \{\hat{\mathbf{P}}_k(\mathbf{T}) > \hat{\mathbf{P}}_{I_\star}(\mathbf{T})\} \\
= \; & \{\hat{\mathbf{P}}_k(\mathbf{T}) > \hat{\mathbf{P}}_{I_\star}(\mathbf{T}), \hat{\mathbf{P}}_{I_\star}(\mathbf{T}) < r_\star - \frac{\epsilon}{2}\} \cup \{\hat{\mathbf{P}}_k(\mathbf{T}) > \hat{\mathbf{P}}_{I_\star}(\mathbf{T}), \hat{\mathbf{P}}_{I_\star}(\mathbf{T}) \geq r_\star - \frac{\epsilon}{2}\},
\end{aligned}
$$

$$
\emptyset = \{\hat{\mathbf{P}}_k(\mathbf{T}) > \hat{\mathbf{P}}_{I_\star}(\mathbf{T}), \hat{\mathbf{P}}_{I_\star}(\mathbf{T}) < r_\star - \frac{\epsilon}{2}\} \cap \{\hat{\mathbf{P}}_k(\mathbf{T}) > \hat{\mathbf{P}}_{I_\star}(\mathbf{T}), \hat{\mathbf{P}}_{I_\star}(\mathbf{T}) \geq r_\star - \frac{\epsilon}{2}\}.
$$

Remark 2 Equality (3.25) comes from the fact that $\{\hat{\mathbf{P}}_k(\mathbf{T}) > \hat{\mathbf{P}}_{I_\star}(\mathbf{T}), \hat{\mathbf{P}}_{I_\star}(\mathbf{T}) \geq r_\star - \frac{\epsilon}{2}\}$ necessarily implies $\{\hat{\mathbf{P}}_k(\mathbf{T}) > r_k + \frac{\epsilon}{2}\}$.

Remark 3 Inequality (3.26) comes from the following relationships

$$
\begin{aligned}
& \{\hat{\mathbf{P}}_k(\mathbf{T}) > \hat{\mathbf{P}}_{I_\star}(\mathbf{T}), \hat{\mathbf{P}}_{I_\star}(\mathbf{T}) < r_\star - \frac{\epsilon}{2}\} \subset \{\hat{\mathbf{P}}_{I_\star}(\mathbf{T}) < r_\star - \frac{\epsilon}{2}\}, \\
& \{\hat{\mathbf{P}}_k(\mathbf{T}) > \hat{\mathbf{P}}_{I_\star}(\mathbf{T}), \hat{\mathbf{P}}_{I_\star}(\mathbf{T}) \geq r_\star - \frac{\epsilon}{2}, \hat{\mathbf{P}}_k(\mathbf{T}) > r_k + \frac{\epsilon}{2}\} \subset \{\hat{\mathbf{P}}_k(\mathbf{T}) > r_k + \frac{\epsilon}{2}\}.
\end{aligned}
$$

Remark 4 Inequality (3.27) is a direct application of the Hoeffding inequality in Lemma 1.

Since there are at most $M-1$ non-ϵ-optimal machine, the probability of selecting a non-ϵ-optimal machine is bounded $2\,(M-1)\exp\left(-(\frac{\epsilon}{2})^2 T\right)$. Therefore, if $T \geq \frac{4}{\epsilon^2}\ln\frac{2(M-1)}{\delta}$, the error probability of choosing non-ϵ-optimal machine is bounded by δ, as desired by the (ϵ,δ)-PAC performance. □

3.2.3 Successive Deletion Algorithm (SDA)

The Successive Deletion Algorithm was proposed in [8]. The underlying idea for SDA is that an inferior machine should be deleted as soon as enough evidence has been collected supporting its inferiority. Owing to its dependence on the testing results, the deletion time of SDA is random instead of deterministic.

We list the structure of SDA here, as proposed in [8].

Successive Deletion Algorithm $(0,\delta)$

Step 1 Set the time index $t=1$, the candidate machine set $\Omega(1)=\{1,\ldots,M\}$ and average reward vector $(\hat{\mathbf{P}}_1(1),\ldots,\hat{\mathbf{P}}_M(1))=(0,\ldots,0)$;

Step 2 If $k\in\Omega(t)$, try machines k and update its average reward $\hat{\mathbf{P}}_k(t)$;

Step 3 Define the threshold to be $\theta(t)=\sqrt{\frac{1}{t}\ln\left(\frac{4Mt^2}{\delta}\right)}$; Find $\hat{\mathbf{P}}_{\max}(t)=\max_{i=1,\ldots,|\Omega(t)|}\hat{\mathbf{P}}_i(t)$; For $\forall\, k\in\Omega(t)$, if $\hat{\mathbf{P}}_{\max}(t)-\hat{\mathbf{P}}_k(t)>2\theta(t)$, then update the candidate machine set $\Omega(t+1)=\Omega(t)\backslash\{k\}$;

Step 4 If $|\,\Omega(t)\,|=1$, then SDA terminates and output the only element in $\Omega(t)$ as our chosen machine I; Otherwise, set $t=t+1$ and go back to **Step 2**.

Remark 1 SDA is a $(0.\delta)$ PAC algorithm. Therefore, SDA's performance satisfies that

$$\mathcal{P}\{\mathcal{E}[\,\mathbf{R}_I\,]=\mathcal{E}[\,\mathbf{R}_{I_*}\,]\}>1-\delta\,. \tag{3.28}$$

where I is SDA's chosen machine and $I_\star$ is the optimal machine. as defined in (3.5).

Remark 2 Simple modification to SDA makes it (ϵ, δ)-PAC, which is proposed in [8].

Owing to its random deletion time, the characterization of SDA's testing complexity is different from that of BDA. Possible alternative approaches include studying SDA's average testing complexity or investigate SDA's testing complexity with high confidence. We adopt the second approach, which is similar to the approach taken in [8], and summarize the main results in the following lemma.

Lemma 3. *The Successive Deletion Algorithm listed above is* $(0, \delta)$*-PAC, i.e. SDA's output satisfies (3.28). Without loss of generality, we assume that the* M *slot machines' average rewards have the following order in amplitude*

$$\boldsymbol{P}_1 \geq \cdots \geq \boldsymbol{P}_M \,.$$

SDA's testing complexity bounded by

$$O\left(\frac{1}{(P_1 - P_2)^2} \ln\left(\frac{1}{(P_1 - P_2)^2}\sqrt{\frac{M}{\delta}}\right) + \sum_{i=2}^{M} \frac{1}{(P_1 - P_i)^2} \ln\left(\frac{1}{(P_1 - P_i)^2}\sqrt{\frac{M}{\delta}}\right)\right), \tag{3.29}$$

with probability at least $1 - \delta$.

Proof. Please refer to **Appendix A** for a detailed derivation. □

Remark Although SDA's testing complexity characterization in (3.29) does not ensure that SDA has better testing complexity than BDA, our simulation verifies that SDA outperforms BDA as far as testing complexity is concerned.

3.2.4 Median Deletion Algorithm (MDA)

The $(\epsilon. \delta)$-SDA has better testing complexity than the (ϵ, δ)-BDA. The reason is that in SDA. the gambler can delete inferior machines at earlier stages, in contrary to BDA. where all the deletions are made at the final time step. However. owing to the random deletion time. to precisely characterize SDA's testing complexity is hard.

Thus, a testing algorithm which encompasses both early deletion and deterministic deletion time is desired. In reference [8]. the authors proposed such an algorithm, under the name Median Deletion Algorithm.

Median Deletion Algorithm (ϵ, δ)

Step 1 When the algorithm starts, we set the stage number $l = 1$, the time index $t = 0$, the candidate machine set $\Omega_1 = \{1, \ldots, M\}$;

Step 2 Update the time index $t = t + T_l$. If machine k belongs to Ω_l, then we try it for T_l times and update its average reward $\hat{\mathbf{P}}_k(t)$.

Step 3 Denote the median of $\{\hat{\mathbf{P}}_k(t), k \in S_l\}$ to be m_l, then we update the candidate machine set as follows: $\Omega_{l+1} = \Omega_l \setminus \{k : \hat{\mathbf{P}}_k(t) < m_l\}$.

Step 4 Update the stage number $l = l + 1$. If $|\Omega_l| = 1$, then MDA terminates and output the only element in Ω_l as our chosen machine I; Otherwise, go back to **Step 2**.

Remark 1 In the above MDA structure, the length of the l^{th} stage is set as follows.

$$T_l = \frac{4}{\epsilon_l^2} \log\left(\frac{3}{\delta_l}\right), \tag{3.30}$$

where ϵ_l and δ_l are pre-configured parameters of MDA's l^{th} stage.

Remark 2 By suitably configuring the parameters ϵ_l, δ_l and T_l, MDA can be made to satisfy the (ϵ, δ)-PAC performance and its complexity is in the order of $O\left(\frac{\log \frac{1}{\delta}}{\epsilon^2} M\right)$. We summarize the main results in the following lemma, which was proved in [8].

Lemma 4. *The Median Deletion Algorithm is* (ϵ, δ)*-PAC if the parameters* $\{\epsilon_l, \delta_l, T_l : l =$

$1, 2, \ldots\}$ *satisfy that*

$$\sum_{i=1}^{\lceil \log_2 M \rceil} \epsilon_l \leq \epsilon, \tag{3.31}$$

$$\sum_{i=1}^{\lceil \log_2 M \rceil} \delta_l \leq \delta. \tag{3.32}$$

and

$$T_l = (\frac{2}{\epsilon_l})^2 \ln\left(\frac{3}{\delta_l}\right) \tag{3.33}$$

There exists parameters settings such that the MDA's testing complexity is in the order of $O\left(\frac{\log(\frac{1}{\delta})}{\epsilon^2} M\right)$.

Remark 1 One possible parameters setting that satisfies the above requirement is proposed in [8],

$$\epsilon_1 = \frac{\epsilon}{4}, \epsilon_{l+1} = \frac{3}{4}\epsilon_l \tag{3.34}$$

$$\delta_1 = \frac{\delta}{2}, \delta_{l+1} = \frac{1}{2}\delta_l \tag{3.35}$$

As long as the worst case testing complexity is concerned, MDA's complexity has the optimal exponent of M among all (ϵ, δ)-PAC algorithm, since it is proved in [9] that the worst case testing complexity of an (ϵ, δ)-PAC algorithm is in the order of $\Theta\left(\frac{\log \frac{1}{\delta}}{\epsilon^2} M\right)$. Therefore, we use a properly configured MDA as our channel testing algorithm.

Chapter 4

Communication System Design

In Chapter 2, we have described the communication scenario to work with and the following communication scheme.

Communication Scheme Structure

1. We segment the time axis into coherence blocks, each of length T_c (Figure 2-1); We also convert the wideband channel into a large number of narrowband subchannels, each of bandwidth W.

2. During each coherence block, the transmitter repeats the following steps.

   Step 1 When the coherence block starts, the transmitter takes M subchannels at random. The transmitter spends E_{te} units of energy in testing these M subchannels with a pre-configured Median Deletion Algorithm (MDA). When MDA terminates, it returns the selected subchannel, denote as subchannel I.

   Step 2 The transmitter then spends the remaining energy in transferring data over the selected subchannel I.

Remark In the above communication scheme. MDA is assumed to be our channel testing algorithm. MDA's parameters need to be pre-configured. The transmitter

doesn't re-configure these parameters along the communication process.

We investigate the above scheme within the framework outlined in Chapter 2.

- The modulation scheme is BPSK with identical constellation $\{+1, -1\}$, for all subchannels and for time.
- Each subchannel experiences a two-level block fading.
- The channel coding can spread over multiple coherence blocks.

The conversion from the wideband channel to the narrowband subchannels is done in such a way that the resulting subchannels are mutually independent. With fixed-level BPSK modulation, each subchannel is represented as a Binary Symmetric Channel (BSC). The two-level fading pattern essentially states that each BSC can be in one of the two states. The crossover probability of a good-state (respectively, a bad-state) BSC is p_G (respectively, p_B), where $0 < p_G < p_B < \frac{1}{2}$. Since channel coding is allowed to spread over multiple coherence blocks, the achievable rate per (informational) symbol for reliable communication is $\mathcal{E}[\, C_{\mathrm{BSC}}(P_I)\,]$, where $\mathcal{E}[\cdot]$ denotes the expectation and $C_{\mathrm{BSC}}(\cdot)$ stands for the BSC capacity.

Our objective is to maximize the data rate by suitably tuning the communication scheme's parameters. Towards this objective, we maximize the achievable rate (ergodic capacity) that can be reliably transferred per coherence block. Since the ergodic capacity is a tight upper bound on the actual data rate, we reasonably expect that the scheme parameters we obtain to improve the ergodic capacity can shed some light on how the parameters should be set to improve the actual data rate.

4.1 Communication Scheme Configuration

As discussed in Chapter 2, we consider the following statistical channel model for each subchannel.

$$\mathbf{y}_l = \mathbf{h}_l\, \mathbf{x}_l + \mathbf{w}_l\,, \tag{4.1}$$

where $\mathbf{h}_l$ denotes the fading coefficient of the l^{th} subchannel. Compared with (2.12), we drop the time index and focus on one input symbol. The two-level fading pattern asserts that $|\mathbf{h}_l|$ can be either h_B or h_G, with probability σ and $1-\sigma$ respectively. Figure 4-1 is a typical plot of the Probability Density Function (PDF) of $|\mathbf{h}_l|$.

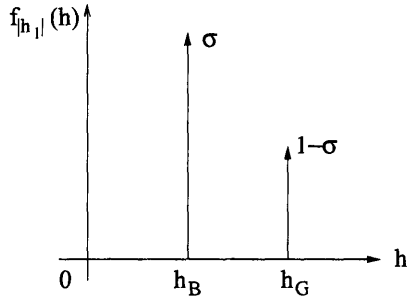

Figure 4-1: PDF of the Fading Coefficient Amplitude $|\mathbf{h}_l|$ in the Two-Level Fading Model

The use of BPSK modulation scheme converts each subchannel to a BSC. We use $\mathbf{P}_l$ to denote the crossover probability of the l^{th} BSC. In (2.20), we related $\mathbf{P}_l$ to $|\mathbf{h}_l|$ as follows,

$$\mathbf{P}_l = Q\left(\frac{|\mathbf{h}_l|}{\sqrt{\frac{N_0}{2}}}\right). \tag{4.2}$$

Owing to the two-level fading pattern, we have the following two possible values for $\mathbf{P}_l$,

$$p_G = Q\left(\frac{h_G}{\sqrt{\frac{N_0}{2}}}\right), \tag{4.3}$$

$$p_B = Q\left(\frac{h_B}{\sqrt{\frac{N_0}{2}}}\right). \tag{4.4}$$

where p_G (respectively, p_B) denotes the crossover probability of the good-state (respectively, bad-state) BSC. The maximal achievable rate of the l^{th} subchannel is the

ergodic capacity of a BSC with crossover probability $\mathbf{P}_l$.

$$\mathbf{C}_l = C_{\mathrm{BSC}}(\mathbf{P}_l)\,, \tag{4.5}$$

$$\text{where} \quad C_{\mathrm{BSC}}(p) = 1 - H_b(p)\,. \tag{4.6}$$

Corresponding to the typical PDF of $\mathbf{h}_l$ in Figure 4-1, we have the following typical plots for the PDFs of $\mathbf{P}_l$ and $\mathbf{C}_l$.

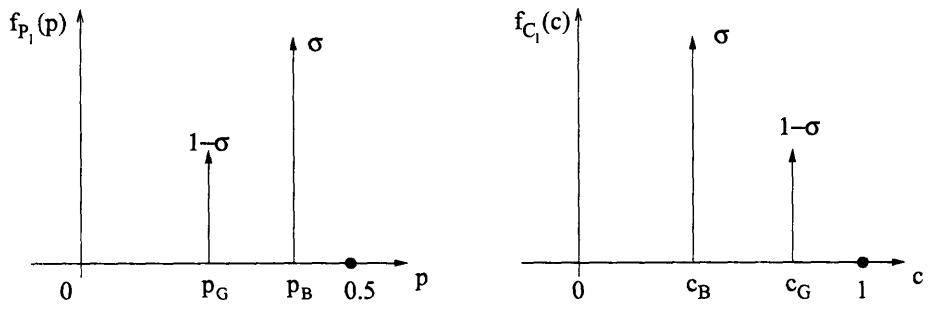

Figure 4-2: PDFs of $\mathbf{P}_l$ and $\mathbf{C}_l$ in the Two-Level Fading Model

The transmitter knows the channel's statistical behavior, i.e. the fading coefficient distribution $f_{|\mathbf{h}_l|}(h)$. Therefore, the transmitter knows the difference between p_B and p_G. However, the transmitter does not know the fading coefficients's actual value. Owing to its greater capacity compared with the bad-state BSC, the good-state BSC is preferable to transmit information-bearing sequence over. Thus, to improve the data rate, the transmitter searches for a good-state BSC during the channel testing phase.

In order to use the results of MABP in Chapter 3, we convert each BSC ($\mathbf{P}$) to a slot machine ($1 - \mathbf{P}$). The conversion method is as follows: *corresponding to a trial on a slot machine, we input a binary symbol into a BSC; if the output symbol of the BSC does not agree with the input symbol, one unit of reward is received; if otherwise, no reward is received.* After the above conversion from BSC to slot machine, looking for a good-state BSC with crossover probability p_G is equivalent to looking for the best slot machine with average reward $1 - p_G$. As we have discussed in Chapter 2, (ϵ, δ) PAC algorithm finds an ϵ-optimal machine with high probability. Therefore, the

transmitter sets $\epsilon = p_B - p_G$, specifies the confidence level δ and constructs the (ϵ, δ) MDA. Finally, he sets up the communication scheme incorporating the constructed (ϵ, δ) MDA as the channel testing algorithm and then runs it on the wideband channel for a long period of time.

4.2 Performance Expression

We list here the MDA's general structure as introduced in Chapter 3.

Median Deletion Algorithm (ϵ, δ)

Preparation Set the current stage index $l = 1$ and the current candidate set $S_1 = \{1, \ldots, M\}$. Compute ϵ_l, δ_l and T_l $(l = 1, \ldots, \lceil \log_2 M \rceil)$ from ϵ and δ.

Step 1 Test each machine k in S_l for T_l times. $\hat{p}_l^k$ denotes the average reward of machine k.

Step 2 Order the machines of S_l according to their average rewards $\hat{p}_l^k$. Denote the median of $\{\hat{p}_l^k, k \in S_l\}$ as m_l. Modify the candidate set S_l by deleting the worse half of it, i.e. $S_{l+1} = S_l \setminus \{k : \hat{p}_k^l < m_l\}$.

Step 3 If $|S_{l+1}| = 1$, MDA terminates and returns the only element of S_{l+1} as the chosen machine I; Otherwise, set $l = l + 1$ and loop back to **Step 1**.

Let $\vec{\mathbf{P}}$ denote $(1 - \mathbf{P}_1, \ldots, 1 - \mathbf{P}_M)$, the converted machines's (from BSCs) average rewards vector. The output of MDA, machine I, satisfies that

$$\mathcal{P}[1 - \mathbf{P}_I = 1 - p_G \,|\, 1 - \mathbf{P}_{I^\star} = 1 - p_G] > 1 - \delta\,, \tag{4.7}$$

$$\text{where} \qquad I^\star = \arg \max_{l=1,\ldots,M} 1 - \mathbf{P}_l\,. \tag{4.8}$$

Let the complexity of a testing algorithm Φ be the number of machine tests, denoted as $\mathbf{T}_\Phi$. We need to estimate MDA's complexity. An upper bound and a lower bound satisfy our needs. Reference [8] proposed and proved the following upper bound on $\mathbf{T}_{\text{MDA}}$.

Lemma 5. *$\boldsymbol{T}_{MDA}$ is upper bounded by $O\left(\frac{M}{\epsilon^2}\ln\frac{1}{\delta}\right)$, i.e. there exists a positive constant C_2 such that*

$$\boldsymbol{T}_{MDA} \;\leq\; C_2\frac{M}{\epsilon^2}\ln\frac{1}{\delta}. \tag{4.9}$$

Proof. Please refer to [8]. □

Remark The upper bound (4.9) does not depend on $\vec{\mathbf{P}}$. Therefore,

$$\mathcal{E}_{\vec{\mathbf{P}}}[\,\mathbf{T}_{\text{MDA}}\,] \;\leq\; C_2\frac{M}{\epsilon^2}\ln\frac{1}{\delta}, \tag{4.10}$$

where $\mathcal{E}_{\vec{\mathbf{P}}}[\cdot]$ denotes the average over all possible average rewards vector $\vec{\mathbf{P}}$.

In addition to the above upper bound on $\mathbf{T}_{\text{MDA}}$ and $\mathcal{E}_{\vec{\mathbf{P}}}[\,\mathbf{T}_{\text{MDA}}\,]$, Reference [9] also proposed and proved the following lower bound on $\mathbf{T}_{\text{MDA}}$.

Lemma 6. *Fix some $\tilde{p}\in(0,\frac{1}{2})$. There exists a positive constant δ_0, and a positive constant $C_0(\tilde{p})$, such that for every $\epsilon\in(0,\frac{1}{2})$, every $\delta\in(0,\delta_0)$, every $\vec{\boldsymbol{P}}\in[0,\frac{1}{2}]^M$, and every (ϵ,δ) PAC algorithm, we have*

$$\mathcal{E}[\,\boldsymbol{T}_{MDA}\,|\,\vec{\boldsymbol{P}}] \;\geq\; C_0(\tilde{p})\left\{\frac{(|M(\vec{\boldsymbol{P}},\epsilon)|-1)^+}{\epsilon^2}+\sum_{l\in N(\vec{\boldsymbol{P}},\epsilon)}\frac{1}{(\boldsymbol{P}_{I^*}-\boldsymbol{P}_l)^2}\right\}\log\frac{1}{8\delta}, \tag{4.11}$$

where, for some positive constant α,

$$M(\vec{\boldsymbol{P}},\epsilon) \;=\; \left\{l:\boldsymbol{P}_l>\boldsymbol{P}_{I^*}-\epsilon,\boldsymbol{P}_l>\tilde{P},\boldsymbol{P}_l\geq\frac{\epsilon+\boldsymbol{P}_{I^*}}{2-\alpha}\right\}. \tag{4.12}$$

$$N(\vec{\boldsymbol{P}},\epsilon) \;=\; \left\{l:\boldsymbol{P}_l\leq\boldsymbol{P}_{I^*}-\epsilon,\boldsymbol{P}_l>\tilde{P},\boldsymbol{P}_l\geq\frac{\epsilon+\boldsymbol{P}_{I^*}}{2-\alpha}\right\}. \tag{4.13}$$

Remark In the two-level fading pattern (Figure 4-2), since we have set ϵ to be $p_B - p_G$, $M(\vec{\mathbf{P}}, \epsilon)$ consists of all the p_G machines and $N(\vec{\mathbf{P}}, \epsilon)$ consists of all the p_B machines. Therefore, we have that

$$\begin{aligned} \mathcal{E}[\,\mathbf{T}_{\mathrm{MDA}}\,] &= \mathcal{E}[\,\mathcal{E}[\,\mathbf{T}_{\mathrm{MDA}}\,|\,\vec{\mathbf{P}}\,]\,] \\ &\geq C_0(1-\sigma^M)\frac{M-1}{\epsilon^2}\log\frac{1}{8\delta} \\ &\geq C_1\frac{M}{\epsilon^2}\log\frac{1}{\delta}\,. \end{aligned} \tag{4.14}$$

for some positive constant C_1.

Owing to the fixed BPSK constellation $\{+1, -1\}$, the complexity $\mathbf{T}$ of the testing algorithm is the same as the energy spent in channel testing, E_{te}. Combining the upper bound (4.9) and the lower bound (4.14),

$$A_1 M \leq \mathcal{E}[\,E_{te}\,] \leq A_2 M\,, \tag{4.15}$$

$$\text{where} \qquad A_1 = \frac{C_1}{\epsilon^2}\log\frac{1}{\delta}\,,$$

$$A_2 = \frac{C_2}{\epsilon^2}\log\frac{1}{\delta}\,.$$

We are now ready to estimate the maximal rate reliably transferred per coherence block, $R(E, M, \sigma)$, for a fixed amount of energy E.

Lemma 7. *Let $R(E, M, \sigma)$ denote the average rate per coherence block. We conclude that $R(E, M, \sigma)$ is bounded from above and from below as follows.*

$$R_l(M, E, \sigma) \leq R(E, M, \sigma) \leq R_u(M, E, \sigma) \tag{4.16}$$

$$R_u(M, E, \sigma) = \max\left\{0, (E - A_1 M)\left[c_B + (c_G - c_B)(1-\sigma^M)\right]\right\} \tag{4.17}$$

$$R_l(M, E, \sigma) = \max\left\{0, (E - A_2 M)\left[c_B + (c_G - c_B)(1-\delta)(1-\sigma^M)\right]\right\} \tag{4.18}$$

Proof. The maximal data rate in a coherence block is the product of $C_{\mathrm{BSC}}(\mathbf{P}_I)$ and the remaining energy $E - E_{te}$ after channel testing. Since coding over many coherence blocks is allowed and the communication system runs for a long time. the maximal

data rate per block is the average of this products.

$$\begin{aligned} R(E, M, \sigma) &= \mathcal{E}[\,(E - E_{te}) C_{\mathrm{BSC}}(\mathbf{P}_I)\,] \\ &= \mathcal{E}[\,(E - E_{te})\,\mathcal{E}[\,C_{\mathrm{BSC}}(\mathbf{P}_I) \mid E_{te}\,]\,] \\ &= \mathcal{E}[\,E - E_{te}\,]\mathcal{E}[\,C_{\mathrm{BSC}}(\mathbf{P}_I)\,]\,. \end{aligned} \tag{4.19}$$

The last step comes from the definition of (ϵ, δ) PAC algorithm. The output of any (ϵ, δ) PAC algorithm satisfies the quality expression in (4.7), which is independent of the testing complexity E_{te}.

We first estimate the ergodic capacity of the chosen BSC I.

$$\begin{aligned} \mathcal{E}[\,C_{\mathrm{BSC}}(\mathbf{P}_I)\,] &= c_B \mathcal{P}[\mathbf{P}_I = p_B] + c_G \mathcal{P}[\mathbf{P}_I = p_G] \\ &= c_B + (c_G - c_B)\mathcal{P}[\mathbf{P}_I = p_G]\,. \end{aligned} \tag{4.20}$$

We use the definition of (ϵ, δ) PAC algorithm to derive a lower bound for $\mathcal{P}[\mathbf{P}_I = p_G]$.

$$\begin{aligned} \mathcal{P}[\{\mathbf{P}_I = p_G\}] &= 1 - \mathcal{P}\,[\{\mathbf{P}_I = p_B\}] \\ &= 1 - \mathcal{P}\,[\{\{\mathbf{P}_{I^*} = p_G\} \cap \{\mathbf{P}_I = p_B\}\} \cup \{\mathbf{P}_{I^*} = p_B\}] \\ &= 1 - (1 - \sigma^M)\,\mathcal{P}\,[\mathbf{P}_I - \mathbf{P}_{I^*} > \varepsilon \,|\, \mathbf{P}_{I^*} = p_G] - \sigma^M \\ &= (1 - \sigma^M)\,(1 - \mathcal{P}\,[\mathbf{P}_I - \mathbf{P}_{I^*} > \varepsilon \,|\, \mathbf{P}_{I^*} = p_G]) \\ &> (1 - \delta)\,(1 - \sigma^M)\,. \end{aligned} \tag{4.21}$$

Step (4.21) follows from the performance expression of the (ϵ, δ) PAC algorithm, (4.7). On the other hand, $\mathcal{P}[\{\mathbf{P}_I = p_G\}]$ is bounded from above as follows.

$$\mathcal{P}[\,\mathbf{P}_I = p_G\,] = (1 - \sigma^M)\,(1 - \mathbb{P}\,[P_I - P_{I^*} > \varepsilon \,|\, P_{I^*} = p_G]) < 1 - \sigma^M\,. \tag{4.22}$$

We have bounded $\mathcal{P}[\{\mathbf{P}_I = p_G\}]$ from above in (4.22) and from below in (4.21).

Hence, lower and upper bounds for $\mathcal{E}[\,C_{\mathrm{BSC}}(\mathbf{P}_I)\,]$ are:

$$\begin{aligned}
\mathcal{E}[\,C_{\mathrm{BSC}}(\mathbf{P}_I)\,] &\leq c_B + (c_G - c_B)(1-\sigma^M)\,, && (4.23)\\
\mathcal{E}[\,C_{\mathrm{BSC}}(\mathbf{P}_I)\,] &\geq c_B + (1-\delta)(c_G - c_B)(1-\sigma^M)\,. && (4.24)
\end{aligned}$$

Combining (4.15), (4.23) and (4.24) into the data rate expression (4.19), we arrive at the desired lower and upper bounds for the data rate $R(M,E,\sigma)$, which denote by R_u and R_l, respectively.

$$\begin{aligned}
R_u(M,E,\sigma) &= \max\left\{0, (E - A_1 M)\left[c_B + (c_G - c_B)(1-\sigma^M)\right]\right\}\,,\\
R_l(M,E,\sigma) &= \max\left\{0, (E - A_2 M)\left[c_B + (c_G - c_B)(1-\delta)(1-\sigma^M)\right]\right\}\,.
\end{aligned}$$

□

4.3 Design of the Communication Scheme

Our objective is to maximize the data rate $R(E,M,\sigma)$ by suitably tuning the the communication scheme parameters. Assuming that the MDA's parameters are fixed, owing to its special structure, the MDA's testing complexity is also fixed. Therefore, we replace the bounds of MDA's testing complexity in (4.15) with the fixed expression of complexity, $A\frac{M}{\epsilon^2}\log\frac{1}{\delta}$. The rate bounds (4.18) and (4.17) reduce to the following expressions.

$$\begin{aligned}
R_l(M,E,\sigma) &\leq R(E,M,\sigma) \leq R_u(M,E,\sigma)\\
R_u(M,E,\sigma) &= \max\left\{0, (E - AM)\left[c_B + (c_G - c_B)(1-\sigma^M)\right]\right\} && (4.25)\\
R_l(M,E,\sigma) &= \max\left\{0, (E - AM)\left[c_B + (c_G - c_B)(1-\delta)(1-\sigma^M)\right]\right\} && (4.26)
\end{aligned}$$

We need to adjust the parameter M, the number of to-test BSCs at the beginning of each coherence block. Although the exact expression of data rate $R(E,M,\sigma)$ is unclear, lower and upper bounds in (4.26) and (4.25) provide us with enough

information to characterize the behavior of the actual rate function, $R(E, M, \sigma)$. Let $M_u^\star$ (respectively, $M_l^\star$) denote the maximizing point for (4.25) (respectively, (4.26)). Since the gap between the upper bound (4.25) and the lower bound (4.26) is negligible as δ approaches 0. their maximizing points $M_u^\star$ and $M_l^\star$ are close to each other as δ approaches 0. Our computation and plot in Figure 4-6 and 4-3 show that the gap between $M_u^\star$ and $M_l^\star$ is indeed negligibly small. Therefore, it is reasonable to choose $M^\star$, the desirable number of BSCs to test at the beginning of each coherence block, between $M_u^\star(\sigma, E)$ and $M_l^\star(\sigma, E)$. Equivalently, we delineate the desirable region for M by $(M_u^\star(\sigma, E), M_l^\star(\sigma, E))$.

Lemma 8. *If $M \in [0, \frac{E}{A}]$, the lower bound $R_l(M, E, \sigma)$ and the upper bound $R_u(M, E, \sigma)$ are both concave in M. The maximizing points of $R_l(M, E, \sigma)$ (respectively $R_u(M, E, \sigma)$), denoted as $M_u^\star(\sigma, E)$ (respectively $M_l^\star(\sigma, E)$), have the following formula*

$$M_l^\star(\sigma, E) = \begin{cases} 0 & \text{if } E \le \frac{Ac_B}{(c_G - c_B)(1-\delta)\ln\frac{1}{\sigma}} \\ \frac{E}{A} + \frac{1 - W_0\left(B_l e^{1+\frac{E}{A}\ln\frac{1}{\sigma}}\right)}{\ln\frac{1}{\sigma}} & \text{if } E > \frac{Ac_B}{(c_G - c_B)(1-\delta)\ln\frac{1}{\sigma}} \end{cases} \tag{4.27}$$

$$M_u^\star(\sigma, E) = \begin{cases} 0 & \text{if } E \le \frac{Ac_B}{(c_G - c_B)\ln\frac{1}{\sigma}} \\ \frac{E}{A} + \frac{1 - W_0\left(B_u e^{1+\frac{E}{A}\ln\frac{1}{\sigma}}\right)}{\ln\frac{1}{\sigma}} & \text{if } E > \frac{Ac_B}{(c_G - c_B)\ln\frac{1}{\sigma}} \end{cases} \tag{4.28}$$

where $B_l = \frac{c_G - \delta(c_G - c_B)}{(1-\delta)(c_G - c_B)}$, $B_u = \frac{c_G}{c_G - c_B}$. $W_0(\cdot)$ denotes the 0^{th} branch of the Lambert function.

Remark For a sketch of the Lambert function, please refer to Figure A-2 in Appendix A.

Proof. It is clear from (4.26) and (4.25) that $R_l(M, E, \sigma)$ and $R_u(M, E, \sigma)$ are zero outside the interval $\left[0, \frac{E}{A}\right]$. Therefore, we focus on the behavior of the two bounds within $\left[0, \frac{E}{A}\right]$. The first and the second derivatives of $R_l(M, E, \sigma)$ and $R_u(M, E, \sigma)$

are summarized here.

$$\begin{aligned}
\frac{dR_l}{dM}(M,E,\sigma) &= -A[c_G + (c_G - c_B)(1-\delta)(1-\sigma^M)] \\
&\quad +(E - A\,M)(c_G - c_B)(1-\delta)\sigma^M \ln\frac{1}{\sigma}\,, \qquad (4.29)\\
\frac{dR_u}{dM}(M,E,\sigma) &= -A[c_G + (c_G - c_B)(1-\sigma^M)] \\
&\quad +(E - A\,M)(c_G - c_B)\sigma^M \ln\frac{1}{\sigma}\,, \qquad (4.30)
\end{aligned}$$

$$\begin{aligned}
\frac{d^2R_l}{dM^2}(M,E,\sigma) &= -2A(c_G - c_B)(1-\delta)\sigma^M \ln\frac{1}{\delta} \\
&\quad -(E - AM)(c_G - c_B)(1-\delta)\sigma^M(\ln\frac{1}{\sigma})^2\,, \qquad (4.31)\\
\frac{d^2R_u}{dM^2}(M,E,\sigma) &= -2A(c_G - c_B)\sigma^M \ln\frac{1}{\sigma} \\
&\quad -(E - AM)(c_G - c_B)\sigma^M(\ln\frac{1}{\sigma})^2\,. \qquad (4.32)
\end{aligned}$$

Clearly, under the condition that $M \in (0, \frac{E}{A})$, $\delta \in (0,1)$ and $\sigma \in (0,1)$, the second derivatives of $R_l(M,E,\sigma)$ and $R_u(M,E,\sigma)$ are negative. Therefore, both $R_l(M,E,\sigma)$ and $R_u(M,E,\sigma)$ are concave in M when $M \in (0, \frac{E}{A})$. A concave function achieves its maximum at the point where its slope vanishes; if the slope does not vanish, the maximum is achieved on the boundary. We notice that

$$\begin{aligned}
\left.\frac{dR_l}{dM}(M,E,\sigma)\right|_{M=\frac{E}{A}} &= -A[c_B + (c_G - c_B)(1-\delta)(1-\sigma^{\frac{E}{A}})]\,, \qquad (4.33)\\
\left.\frac{dR_u}{dM}(M,E,\sigma)\right|_{M=\frac{E}{A}} &= -A[c_B + (c_G - c_B)(1-\sigma^{\frac{E}{A}})]\,. \qquad (4.34)
\end{aligned}$$

are both negative. Therefore, the location of $M_l^\star(\sigma,E)$ (respectively, $M_u^\star(\sigma,E)$) de-

pends on the sign of $\frac{dR_l}{dM}(M,E,\sigma)\big|_{M=0}$ (respectively, $\frac{dR_u}{dM}(M,E,\sigma)\big|_{M=0}$).

$$M_l^\star(\sigma,E) = \begin{cases} 0 & \text{if } \frac{dR_l}{dM}(M,E,\sigma)\big|_{M=0} \le 0 \\ \frac{E}{A} + \frac{1-W_0\left(B_l e^{1+\frac{E}{A}\ln\frac{1}{\sigma}}\right)}{\ln\frac{1}{\sigma}} & \text{if } \frac{dR_l}{dM}(M,E,\sigma)\big|_{M=0} > 0 \end{cases} \tag{4.35}$$

$$M_u^\star(\sigma,E) = \begin{cases} 0 & \text{if } \frac{dR_u}{dM}(M,E,\sigma)\big|_{M=0} \le 0 \\ \frac{E}{A} + \frac{1-W_0\left(B_u e^{1+\frac{E}{A}\ln\frac{1}{\sigma}}\right)}{\ln\frac{1}{\sigma}} & \text{if } \frac{dR_u}{dM}(M,E,\sigma)\big|_{M=0} > 0 \end{cases} \tag{4.36}$$

Substituting the expressions of $\frac{dR_l}{dM}(M,E,\sigma)\big|_{M=0}$ and $\frac{dR_u}{dM}(M,E,\sigma)\big|_{M=0}$, we arrive at the following desired formula.

$$M_l^\star(\sigma,E) = \begin{cases} 0 & \text{if } E \le \frac{Ac_B}{(c_G-c_B)(1-\delta)\ln\frac{1}{\sigma}} \\ \frac{E}{A} + \frac{1-W_0\left(B_l e^{1+\frac{E}{A}\ln\frac{1}{\sigma}}\right)}{\ln\frac{1}{\sigma}} & \text{if } E > \frac{Ac_B}{(c_G-c_B)(1-\delta)\ln\frac{1}{\sigma}} \end{cases}, \tag{4.37}$$

$$M_u^\star(\sigma,E) = \begin{cases} 0 & \text{if } E \le \frac{Ac_B}{(c_G-c_B)\ln\frac{1}{\sigma}} \\ \frac{E}{A} + \frac{1-W_0\left(B_u e^{1+\frac{E}{A}\ln\frac{1}{\sigma}}\right)}{\ln\frac{1}{\sigma}} & \text{if } E > \frac{Ac_B}{(c_G-c_B)\ln\frac{1}{\sigma}} \end{cases}. \tag{4.38}$$

□

Although (4.27) and (4.28) provide the exact formula for $M_u^\star(\sigma,E)$ and $M_l^\star(\sigma,E)$, they obscure the clear relationship between $M^\star$ and E, in which we are more interested and which is easier to use in practice. Towards this objective, we simplify the exact expression in (4.27) and (4.28) through approximation and summarize the main results in the following lemma.

Lemma 9. *$M_u^\star$ (respectively, $M_l^\star$) as in (4.28) (respectively, (4.27)) has following approximation, which is a logarithmic function in E.*

(1) When $E \gg \frac{Ac_B}{(c_G-c_B)\ln\frac{1}{\sigma}}$,

$$M_u^\star(\sigma,E) = \log_{\frac{1}{\sigma}}\left(\frac{1+\ln B_u}{B_u} + \left(\frac{\ln\frac{1}{\sigma}}{AB_u}\right)E\right).$$

where $B_u = \frac{c_G}{(c_G - c_B)}$.

(2) When $E \gg \frac{Ac_B}{(c_G - c_B)(1-\delta)\ln\frac{1}{\sigma}}$,

$$M_l^\star(\sigma, E) \;=\; \log_{\frac{1}{\sigma}}\left(\frac{1+\ln B_l}{B_l} + \left(\frac{\ln\frac{1}{\sigma}}{AB_l}\right)E\right),$$

where $B_l = \frac{c_G - \delta(c_G - c_B)}{(1-\delta)(c_G - c_B)}$.

Proof. The 0^{th} branch of the Lambert function has the following approximation as z goes to $+\infty$.

$$W_0(z) \;=\; \ln z - \ln\ln z + O\left[\left(\frac{\ln\ln z}{\ln z}\right)\right]. \tag{4.39}$$

By applying the above approximation (4.39) to the following expressions of $M_u^\star(\sigma, E)$ and $M_l^\star(\sigma, E)$,

$$M_l^\star(\sigma, E) \;=\; \begin{cases} 0 & \text{if } E \le \frac{Ac_B}{(c_G - c_B)(1-\delta)\ln\frac{1}{\sigma}} \\ \frac{E}{A} + \frac{1 - W_0\left(B_l e^{1+\frac{E}{A}\ln\frac{1}{\sigma}}\right)}{\ln\frac{1}{\sigma}} & \text{if } E > \frac{Ac_B}{(c_G - c_B)(1-\delta)\ln\frac{1}{\sigma}} \end{cases} \tag{4.40}$$

$$M_u^\star(\sigma, E) \;=\; \begin{cases} 0 & \text{if } E \le \frac{Ac_B}{(c_G - c_B)\ln\frac{1}{\sigma}} \\ \frac{E}{A} + \frac{1 - W_0\left(B_u e^{1+\frac{E}{A}\ln\frac{1}{\sigma}}\right)}{\ln\frac{1}{\sigma}} & \text{if } E > \frac{Ac_B}{(c_G - c_B)\ln\frac{1}{\sigma}} \end{cases} \tag{4.41}$$

we arrive at the following desired simple approximation for (4.27).

$$M_l^\star(\sigma, E) \;=\; \log_{\frac{1}{\sigma}}\left(\frac{1+\ln B_l}{B_l} + \left(\frac{\ln\frac{1}{\sigma}}{AB_l}\right)E\right),$$

which is precise when $E \gg \frac{Ac_B}{(c_G - c_B)(1-\delta)\ln\frac{1}{\sigma}}$.

Similarly, we get the following desired simple approximation for (4.28).

$$M_u^\star(\sigma, E) \;=\; \log_{\frac{1}{\sigma}}\left(\frac{1+\ln B_u}{B_u} + \left(\frac{\ln\frac{1}{\sigma}}{AB_u}\right)E\right)$$

which is precise when $E \gg \frac{Ac_B}{(c_G - c_B)\ln\frac{1}{\sigma}}$. □

Now, we draw several plots to understand how of $M_u^\star(\sigma, E)$ and $M_l^\star(\sigma, E)$ behave as E varies. The parameters of the scenario we study are

$$p_G = 0.1, \quad p_B = 0.45, \quad \delta = 0.1, \quad \sigma = 0.95\,.$$

Figure 4-3 illustrates How $M_u^\star$ and $M_l^\star$ behave as E varies from 0 to 4×10^6. The curve with "+" is for $M_l^\star$ and the one with "o" is for $M_u^\star$. The curves illustrate the logarithmic relationship between $M_u^\star$, $M_l^\star$ and E. The difference between the two curves is almost invisible, owing to the fact that the gap between $M_u^\star$ and $M_l^\star$ is negligible compared with the range of $M_u^\star$ and $M_l^\star$.

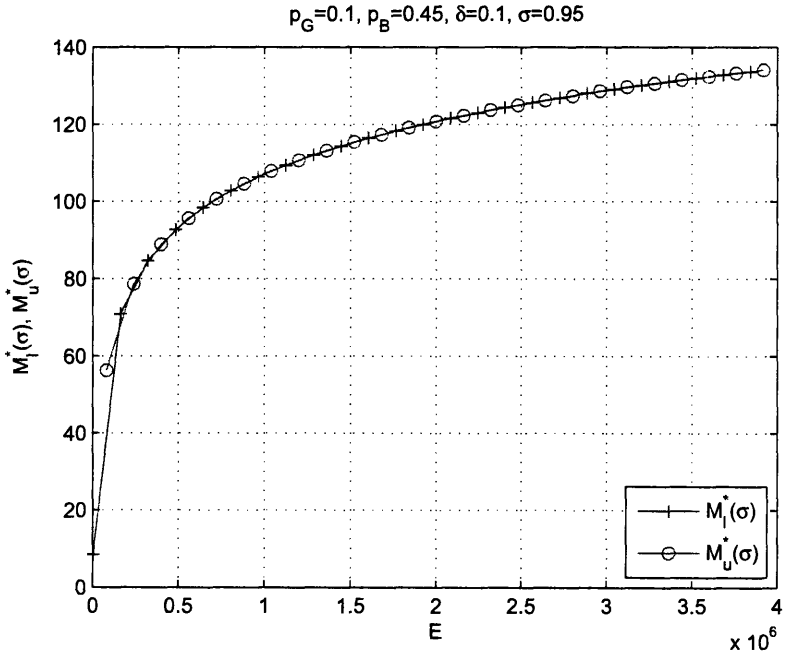

Figure 4-3: For a fixed σ, how $M_u^\star$ and $M_l^\star$ behave as E varies between 0 and 4×10^6. The logarithmic relationship can be clearly seen.

To illustrate the small difference between the two curves, we expand the upper-right corner of the Figure (4-3) in Figure (4-4). In this plot, the gap between $M_u^\star$ and $M_l^\star$ is still small, but visible. Note that we have already intentionally made $\delta = 0.95$ not too close to 0, so that the difference between $M_u^\star(\sigma, E)$ and $M_l^\star(\sigma, E)$ can possibly be visible.

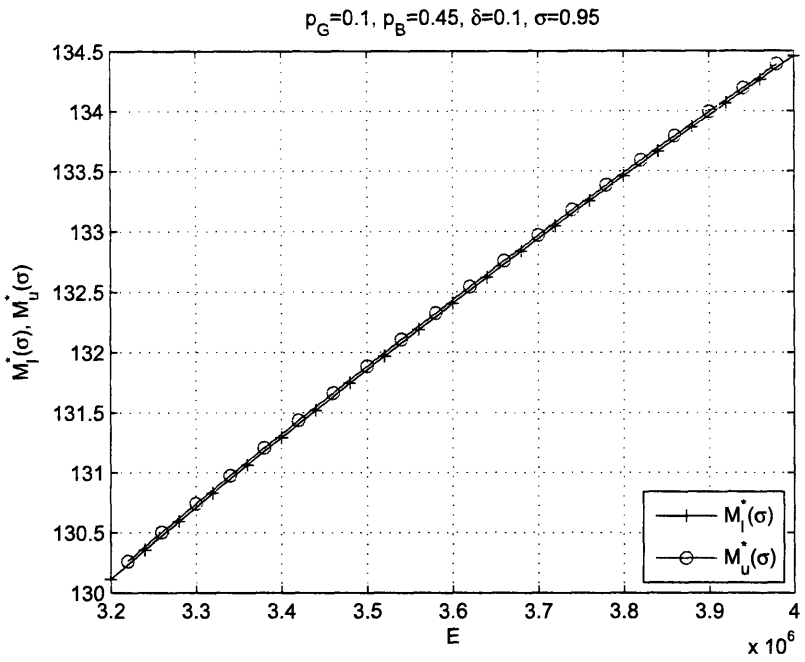

Figure 4-4: Expanded upper right corner of Figure 4-3, where E varies between 3.2×10^6 and 4×10^6, the difference between the two curves are visible.

Actually, since the upper and the lower bounds are so close to each other in most scenarios, as illustrated in the above figures, they may well be treated as approximation to rather than bounds on the desirable number of probed subchannels.

4.4 Discussion

4.4.1 Integer Constraint on the Subchannel Number

One component we haven't yet considered in the above procedure is the integer constraint on M. Since it is meaningless to have a fraction of BSC, we need to deal with the case of non-integer $M^\star$. For non-integer $M^\star$. we can always find two consecutive integers M_0, M_1 such that,

$$M_0 < M^\star < M_1 \text{ and } M_0 + 1 = M_1 .$$

Now $M^\star$ can be expressed as a linear combination of M_0 and M_1, by solving the following linear equation system for $q_0, q_1 \in (0,1)$,

$$\begin{aligned} M^\star &= q_0 M_0 + q_1 M_1 \,, \\ 1 &= q_0 + q_1 \,. \end{aligned}$$

Then we modify the communication scheme: at the beginning of each coherence block, we flip a coin with "Head" probability q_0 and "Tail" probability q_1; if we get a "Head", the parameter M is set to be M_0 and if otherwise, M is set to be M_1; then we carry out the original communication scheme in that coherence block. Owing to the concavity of $R_l(M,E,\sigma)$ (respectively, $R_u(M,E,\sigma)$), this method of mixing M_0 and M_1 to generate M results in the data rate that is closest to $R_l(M_l^\star,E,\sigma)$ (respectively, $R_u(M_u^\star,E,\sigma)$) under the integer constraint on M. Now, we have a unified solution to the problem with or without the integer constraint on M.

4.4.2 Impact of Channel Quality

We are also interested in how $M^\star$ behaves as σ varies within the interval $(0,1)$. According to Figure 4-1 and 4-2, σ represents the probability of a subchannel being in the "bad" state. Therefore, for fixed h_B and h_G (and thus fixed p_B, p_G, c_B and c_G), the larger the σ is, the worse the subchannel is. Thus, we are interested in how the channel quality impacts the tradeoff between channel testing and data transmission.

We have the slope of $M_u^\star(\sigma,E)$ and $M_l^\star(\sigma,E)$ to σ as follows.

$$\begin{aligned} \frac{dM_u^\star(\sigma,E)}{d\sigma} &= \frac{1}{\sigma \ln\left(\frac{1}{\sigma}\right)} \left(\frac{1 - W\left(D_u(\sigma,E)\right)}{\ln\left(\frac{1}{\sigma}\right)} + \frac{E}{A} \frac{W\left(D_u(\sigma,E)\right)}{1 + W\left(D_u(\sigma,E)\right)} \right) , \\ \frac{dM_l^\star(\sigma,E)}{d\sigma} &= \frac{1}{\sigma \ln\left(\frac{1}{\sigma}\right)} \left(\frac{1 - W\left(D_l(\sigma,E)\right)}{\ln\left(\frac{1}{\sigma}\right)} + \frac{E}{A} \frac{W\left(D_l(\sigma,E)\right)}{1 + W\left(D_l(\sigma,E)\right)} \right) , \end{aligned}$$

where. $W(\cdot)$ is the Lambert function and

$$\begin{aligned} D_u(\sigma, E) &= \frac{c_G}{c_G - c_B} e^{1+\frac{E}{A}\ln\left(\frac{1}{\sigma}\right)}, \\ D_l(\sigma, E) &= \frac{c_G - \delta(c_G - c_B)}{(1-\delta)(c_G - c_B)} e^{1+\frac{E}{A}\ln\left(\frac{1}{\sigma}\right)}. \end{aligned}$$

Lemma 10. *When σ is close to 0, $M_u^\star(\sigma, E)$ and $M_l^\star(\sigma, E)$ increase with σ; However, when σ is close to 1, $M_u^\star(\sigma, E)$ and $M_l^\star(\sigma, E)$ decrease with σ.*

Proof. First, we study the slopes of $M_u^\star(\sigma, E)$ and $M_l^\star(\sigma, E)$ when σ is close to 0.

$$\begin{aligned} &\lim_{\sigma\to 0} \frac{dM_u^\star(\sigma, E)}{d\sigma} \\ &= \lim_{\sigma\to 0} \frac{\left(\frac{1 - W\left(\frac{c_G}{c_G - c_B} e^{\left(1+\frac{E}{A}\ln\left(\frac{1}{\sigma}\right)\right)}\right)}{\ln\left(\frac{1}{\sigma}\right)} + \frac{E}{A} \frac{W\left(\frac{c_G}{c_G - c_B} e^{\left(1+\frac{E}{A}\ln\left(\frac{1}{\sigma}\right)\right)}\right)}{1 + W\left(\frac{c_G}{c_G - c_B} e^{\left(1+\frac{E}{A}\ln\left(\frac{1}{\sigma}\right)\right)}\right)} \right)}{\ln\left(\frac{1}{\sigma}\right)} \qquad (4.42) \\ &= \lim_{\sigma\to 0} \frac{\left(\frac{1 - \left(\ln\left(\frac{c_G}{c_G - c_B} e^{\left(1+\frac{E}{A}\ln\left(\frac{1}{\sigma}\right)\right)}\right) - \ln\ln\left(\frac{c_G}{c_G - c_B} e^{\left(1+\frac{E}{A}\ln\left(\frac{1}{\sigma}\right)\right)}\right)\right)}{\ln\left(\frac{1}{\sigma}\right)} + \frac{E}{A} \right)}{\ln\left(\frac{1}{\sigma}\right)} \qquad (4.43) \\ &= \lim_{\sigma\to 0} \frac{\ln\ln\left(\frac{c_G}{c_G - c_B} e^{\left(1+\frac{E}{A}\ln\left(\frac{1}{\sigma}\right)\right)}\right) - \ln\frac{c_G}{c_G - c_B}}{\left(\ln\left(\frac{1}{\sigma}\right)\right)^2} > 0. \qquad (4.44) \end{aligned}$$

In Step (4.43), we use the following facts

$$W\left(\frac{c_G}{c_G - c_B} e^{\left(1+\frac{E}{A}\ln\left(\frac{1}{\sigma}\right)\right)}\right) \to +\infty, \qquad \text{as } \sigma \to 0^+,$$

$$W(z) \doteq \ln z - \ln\ln z, \qquad \text{as } z \to +\infty.$$

By carrying out steps similar to (4.42-4.44), we can also show that

$$\lim_{\sigma\to 0} \frac{dM_l^\star(\sigma, E)}{d\sigma} > 0.$$

To show that $M_u^\star(\sigma, E)$ and $M_l^\star(\sigma, E)$ decrease as σ gets close to 1, we study the

behavior of their slopes near $\sigma = 1$ as follows.

$$\begin{aligned}
&\lim_{\sigma\to 1} \frac{dM_u^\star(\sigma, E)}{d\sigma} \\
&= \lim_{\sigma\to 1} \frac{1}{\ln\left(\frac{1}{\sigma}\right)} \left(\frac{1 - W\left(\frac{c_G e}{c_G - c_B}\right)}{\ln\left(\frac{1}{\sigma}\right)} + \frac{E}{A} \frac{W\left(\frac{c_G e}{c_G - c_B}\right)}{1 + W\left(\frac{c_G e}{c_G - c_B}\right)} \right) \\
&= \lim_{\sigma\to 1} \frac{1}{\ln\left(\frac{1}{\sigma}\right)} \left(\frac{1 - W\left(\frac{c_G e}{c_G - c_B}\right)}{\ln\left(\frac{1}{\sigma}\right)} \right) < 0, \qquad (4.45)
\end{aligned}$$

where the last step follows from $W\left(\frac{c_G e}{c_G - c_B}\right) > 1$.

Similarly

$$\begin{aligned}
&\lim_{\sigma\to 1} \frac{dM_l^\star(\sigma, E)}{d\sigma} \\
&= \lim_{\sigma\to 1} \frac{1}{\ln\left(\frac{1}{\sigma}\right)} \left(\frac{1 - W\left(\frac{(c_G - \delta(c_G - c_B))e}{(1-\delta)(c_G - c_B)}\right)}{\ln\left(\frac{1}{\sigma}\right)} + \frac{E}{A} \frac{W\left(\frac{(c_G - \delta(c_G - c_B))e}{(1-\delta)(c_G - c_B)}\right)}{1 + W\left(\frac{(c_G - \delta(c_G - c_B))e}{(1-\delta)(c_G - c_B)}\right)} \right) \\
&= \lim_{\sigma\to 1} \frac{1}{\ln\left(\frac{1}{\sigma}\right)} \left(\frac{1 - W\left(\frac{(c_G - \delta(c_G - c_B))e}{(1-\delta)(c_G - c_B)}\right)}{\ln\left(\frac{1}{\sigma}\right)} \right) < 0, \qquad (4.46)
\end{aligned}$$

where the last step comes from $W\left(\frac{(c_G - \delta(c_G - c_B))e}{(1-\delta)(c_G - c_B)}\right) > 1$. □

Remark 1 We have the following interpretation for the lemma. For a fixed amount of energy,

- When the subchannel quality is good (i.e. σ is close to 0), more energy should be allocated to channel testing ($M^\star$ increases) as the subchannel grows worse (σ increases). The reason is that the transmitter still has a hope of finding a good subchannel by testing more subchannels.

- However, when the subchannel quality is bad (i.e. σ is close to 1), less energy should be allocated to channel testing ($M^\star$ decreases) as the subchannel grows worse (σ increases). Here, the reason is that the transmitter does not expect to find a good subchannel, since σ is too close to 1.

Finally, we make several plots for the typical case where $p_G = 0.1, p_B = 0.45, \delta = 0.01$.

- Fix $E = 1 \times 10^3$. plot $M_u^\star$ and $M_l^\star$ for various $\sigma \in (0.1)$. Figure 4-5 clearly illustrates the lemma.

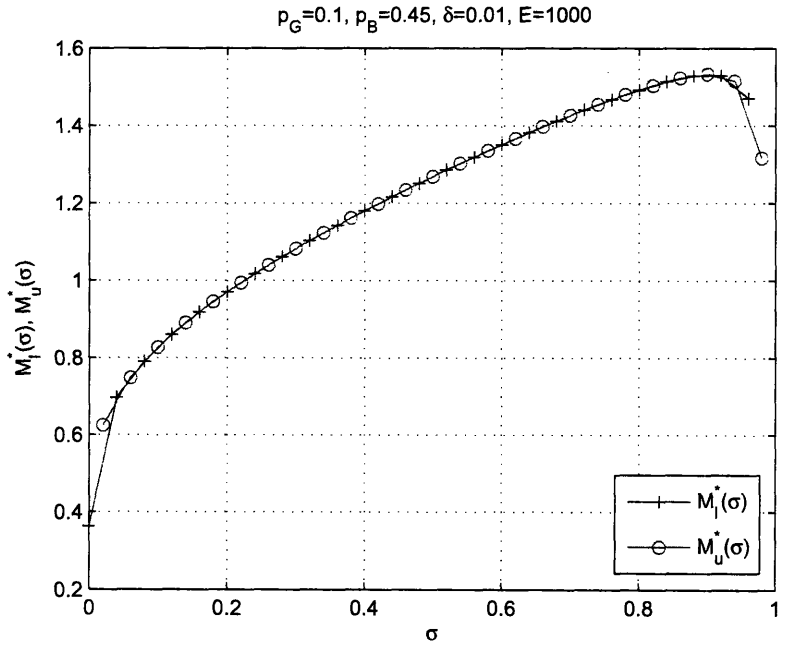

Figure 4-5: How $M_l^\star$ and $M_u^\star$ behave as σ varies (for a fixed small E)

- Fix $E = 1 \times 10^4$, plot $M_u^\star$ and $M_l^\star$ for various $\sigma \in (0, 1)$. At the first glance, Figure 4-6 does not agree with the previous lemma. The reason for this seeming discrepancy is that the turning point in Figure 4-5 is so close to 1 that it is not illustrated in this figure. To verify that the turning point does exist in this case, we expand the upper right corner of Figure 4-6 in Figure 4-7, in which the turning point can be easily seen.

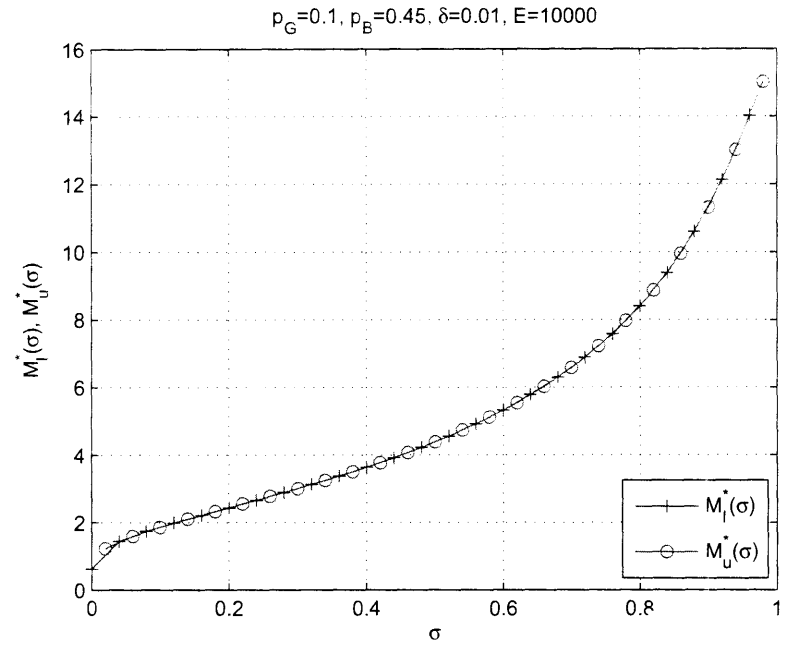

Figure 4-6: How $M_l^\star$ and $M_u^\star$ behave as σ varies (for a fixed large E)

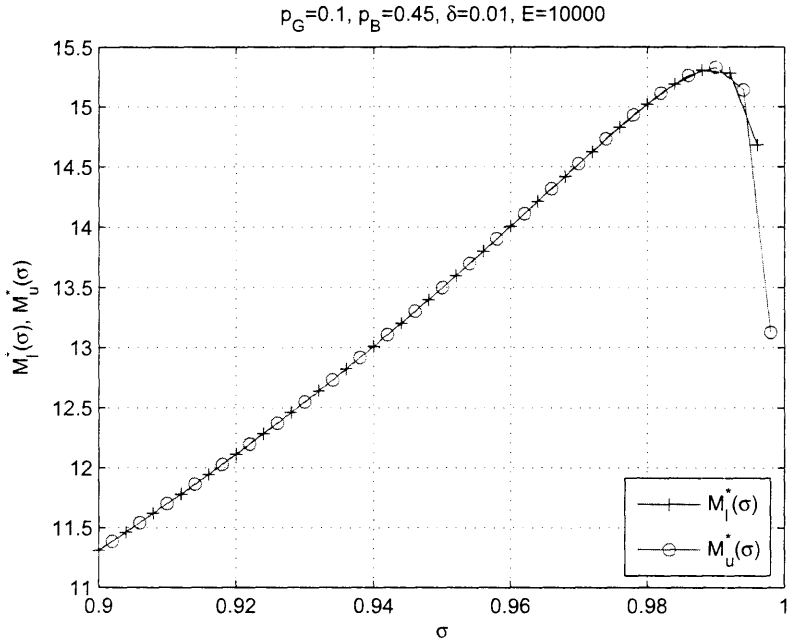

Figure 4-7: Expanded Upper Right corner of Figure 4-6. where the turning points of both curves are explicitly shown

Chapter 5

Conclusions and Future Directions

5.1 Conclusions

As stated in the introduction chapter, the main objective of this thesis is to achieve higher data rates over a wideband block fading channel in the low SNR scenario. Owing to the lack of the sender's CSI, we employ a testing-transmission scheme. To efficiently use the limited amount of energy, we need to balance the energy consumption between channel testing and data transmission. By converting the wideband channel to multiple narrowband subchannels and using BPSK signaling, we reduce the above energy tradeoff problem to the problem of finding the desirable number of tested subchannels. A desirable region was found in Chapter 4 for the number of tested subchannels. Moreover, in Chapter 4, we also studied how this region evolves as the energy constraint and the channel quality vary, respectively. The main results are summarized as follows,

- If the channel quality level is fixed, then the desirable number of tested subchannels increases as a logarithmic function of the available energy (Lemma 9);

- If the amount of available energy is fixed and the channel quality level is close to the good state, then the desirable number of tested subchannels increases as the channel quality level increases (Lemma 10);

- If the amount of available energy is fixed and the channel quality level is close to the bad state, then the desirable number of tested subchannels decreases as the channel quality level increases (Lemma 10);

These results characterize a desirable region for the number of probed subchannels given the block energy constraint and the channel quality level. The upper bound and the lower bound, which specify this region, are so close to each other that they may well be regarded as an approximation to the desirable number of probed subchannels. Consequently, with the communication structure described in Chapter 2 and Chapter 3, we are able to carry out the communication over the wideband channel and expect desirable data rates.

5.2 Future Directions

One of the main contributions of this thesis is the new problem formulation, which leave many open questions to be solved in the future research, part of them are listed here,

- The results obtained in the two level fading model in this thesis can be extended to more general fading models, including multiple level fading model;
- The results obtained for single user communication in this thesis can guide future investigations into the Multiple Access Channel.

Appendix A

Proof of Lemma 3

We list Lemma 3 here for convenience.

Without loss of generality, we assume that the M reward machines are ordered such that $P_1 \geq \cdots \geq P_M$. The Successive Deletion Algorithm is $(0, \delta)$-PAC. Its testing complexity is $O\left(\frac{1}{(P_1-P_2)^2} \ln\left(\frac{1}{(P_1-P_2)^2}\sqrt{\frac{M}{\delta}}\right) + \sum_{i=2}^{M} \frac{1}{(P_1-P_i)^2} \ln\left(\frac{1}{(P_1-P_i)^2}\sqrt{\frac{M}{\delta}}\right)\right)$, with probability at least $1-\delta$.

As we have mentioned in Chapter 3, the deletion time points of inferior machines are random rather than fixed. We begin our investigation of the Successive Deletion Algorithm's complexity by studying the simple two-machine case.

A.1 Two-Machine Case

In the two-machine case, we need to make a decision between machine 1 and machine 2. Initially, the candidate machine set $\Omega(0)$ consists of machine 1 and machine 2. Let the testing score for machine l at time t be $R_l(t)$, where $l \in \{1, 2\}$. We use P_l to denote the average reward of the l^{th} machine. We now define the cumulative score and the average score at time t to be $S_l(t) = \sum_{k=1}^{t} R_l(k)$ and $\hat{P}_l(t) = \frac{S_l(t)}{t}$, where $l \in \{1.2\}$. We use $\hat{P}_{\max}(t) = \max_l \hat{P}_l(t)$ to denote the maximal average reward at time t. In the Successive Deletion Algorithm, we calculate the difference between the

maximal average score $\hat{P}_{\max}(t)$ and each machine's average score $\hat{P}_l(t)$ and compare it with twice the threshold $\theta(t) = \sqrt{\frac{1}{t}\ln(\frac{8}{\delta}t^2)}$. If the difference is larger than $2\theta(t)$, the machine with smaller average score is deleted from the candidate set and never considered again. The Successive Deletion Algorithm terminates when the candidate set consists of only one machine, which is the result to be returned by the algorithm. Clearly, one deletion suffices for the two-machine case. It is shown in [8] that the event $\left\{ |p_l - \hat{P}_l(t)| \leq \theta(t), t \in \mathbb{N}^+, l = 1, 2 \right\}$ occurs with probability at least $1 - \delta$. We will focus on this typical event in the following derivation. Since the threshold $\theta(t)$ is decreasing with t, the average score $\hat{P}_l(t)$ of each machine is increasingly confined to the neighborhood of its average reward P_l. Thus, the inferior machine will eventually be deleted and an upper bound can be derived for the deletion time. Without loss of generality, we assume that machine 1 has smaller average reward P_1. Let Δ denote $|p_1 - p_2|$. We illustrate how to bound the deletion time from above with the following figure.

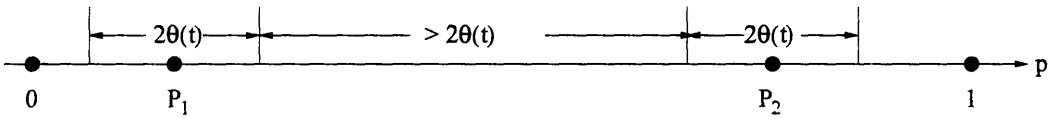

Figure A-1: Sufficient Condition for the Successive Deletion Algorithm to Delete the Inferior Machine (with average reward p_1) in the two-machine case.

As shown in Figure A-1, the condition $4\theta(t) \leq \Delta$ implies that $\hat{P}_2(t) - \hat{P}_1(t) \geq 2\theta(t)$. According to SDA, at time t, machine 1 must be deleted, since

$$\hat{P}_{\max}(t) - \hat{P}_1(t) \geq \hat{P}_2(t) - \hat{P}_1(t) \geq 2\theta(t)\,. \tag{A.1}$$

Therefore, the deletion time of machine 1 must be earlier than the solution of $4\theta(t) = \Delta$. We list all the three solutions for $4\theta(t) = \Delta$ here.

$$t_1(\Delta, \delta) = -\frac{32}{\Delta^2} W_{-1}\left(-\frac{\Delta^2}{128}\sqrt{2\delta}\right) \quad (A.2)$$

$$t_2(\Delta, \delta) = -\frac{32}{\Delta^2} W_0\left(-\frac{\Delta^2}{128}\sqrt{2\delta}\right) \quad (A.3)$$

$$t_3(\Delta, \delta) = -\frac{32}{\Delta^2} W_0\left(\frac{\Delta^2}{128}\sqrt{2\delta}\right) \quad (A.4)$$

where $W_k(\cdot)$ stands for the k^{th} branch of the Lambert W function. In Figure A-2, we make a plot of the $(-1)^{\text{th}}$ and the 0^{th} branch of the Lambert W function.

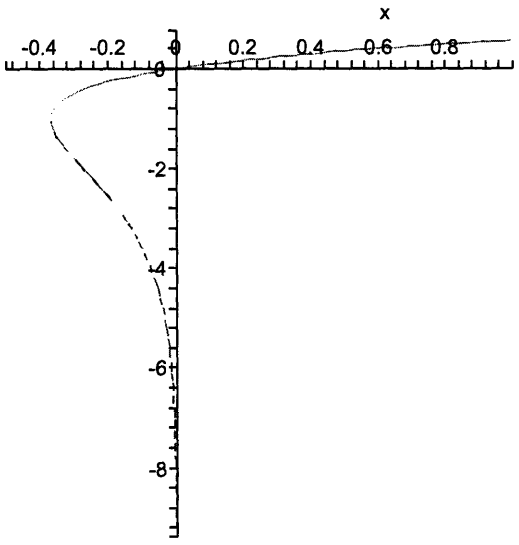

Figure A-2: The $(-1)^{\text{th}}$ and the 0^{th} branch of the Lambert W function. The upper solid part of the curve is the 0^{th} branch, $W_0(z)$, and the lower dash part is the $(-1)^{\text{th}}$ branch, $W_{-1}(z)$.

Now, we need to find out, among (A.2), (A.3) and (A.4), the true upper bound on the deletion time.

Clearly, $t_3(\Delta, \delta)$ can not be the upper bound we are looking for, since it is negative. For $t_1(\Delta, \delta)$ and $t_2(\Delta, \delta)$, the input to the Lambert W function is $-\frac{\Delta^2}{128}\sqrt{2\delta}$, which belongs to the interval $(-e^{-1}, 0)$ (since $\Delta \in (0, \frac{1}{2}]$ and $\delta \in (0, 1]$). Therefore, we

will focus on the negative part of the Lambert W function $W_{-1}(z)$ and $W_0(z)$. where $z < 0$. In Figure A-2, we notice that the two branches of the Lambert W function $W_{-1}(z)$ and $W_0(z)$ both exist for $-e^{-1} \leq z < 0$, rendering the Lambert W function a multi-value function in this interval.

Now, we set out to show that $t_2(\Delta, \delta)$ can not be a proper upper bound on the deletion time we are looking for. Our objective is to show that

$$\max_{\delta \in (0, \frac{1}{2}], \Delta \in (0,1]} t_2(\Delta, \delta) < 1\,, \tag{A.5}$$

which naturally tells us that $t_2(\Delta, \delta)$ is not a proper upper bound.

Clearly, $t_2(\Delta, \delta)$ is an increasing function of δ, in the interval $\delta \in (0, \frac{1}{2}]$. Therefore, for a fixed $\Delta \in (0, \frac{1}{2}]$, $t_2(\Delta, \delta)$ achieves its maximum at $\delta = 1$.

$$\begin{aligned} & \max_{\delta \in (0,1], \Delta \in (0, \frac{1}{2}]} t_2(\Delta, \delta) \\ = & \max_{\Delta \in (0, \frac{1}{2}]} \max_{\delta \in (0,1]} t_2(\Delta, \delta) \\ = & \max_{\Delta \in (0, \frac{1}{2}]} t_2(\Delta, \delta)|_{\delta=1} \\ = & \max_{\Delta \in (0, \frac{1}{2}]} -\frac{32}{\Delta^2} W_0\left(-\frac{\sqrt{2}\Delta^2}{128}\right). \end{aligned} \tag{A.6}$$

Then, since

$$\frac{d\left(-\frac{32}{\Delta^2} W_0\left(-\frac{\sqrt{2}\Delta^2}{128}\right)\right)}{d\Delta} = \frac{64\, W_0^2\left(-\frac{\sqrt{2}\Delta^2}{128}\right)}{\Delta^3\left(1 + W_0\left(-\frac{\sqrt{2}\Delta^2}{128}\right)\right)} > 0 \quad \text{for } \forall \Delta \in (0, \frac{1}{2}]$$

and

$$\lim_{\Delta \to 0^+} t_2(\Delta, \delta)|_{\delta=1} = \lim_{\Delta \to 0^+} -\frac{32}{\Delta^2} W_0\left(-\frac{\sqrt{2}\Delta^2}{128}\right) = \frac{\sqrt{2}}{4} < 1$$

$$t_2(\Delta, \delta)|_{\Delta=\frac{1}{2}, \delta=1} = -32 W_0(-\frac{\sqrt{2}}{512}) < 1\,.$$

therefore,

$$\begin{aligned} & \max_{\delta\in(0,1],\Delta\in(0,\frac{1}{2}]} t_2(\Delta,\delta) \\ = & \max_{\Delta\in(0,\frac{1}{2}]} -\frac{32}{\Delta^2} W_0\left(-\frac{\sqrt{2}\Delta^2}{128}\right) \\ < & 1\,. \end{aligned}$$

We conclude that $t_2(\Delta,\delta)$ takes value in $[0,1)$ and can not be a proper upper bound on the deletion time. Thus, $t_1(\Delta,\delta)$ in (A.2) is the correct upper bound on the deletion time.

Finally, we need an approximation formula for the upper bound, $t_1(\Delta,\delta) = -\frac{32}{\Delta^2} W_{-1}\left(-\frac{\Delta^2}{128}\sqrt{2\delta}\right)$. As z approaches 0^-, $W_{-1}(z)$ can be approximated by the following asymptotic series expansion (by Lagrange Inversion Theorem).

$$W_{-1}(z) = L_1 - L_2 + \sum_{l=0}^{+\infty}\sum_{m=1}^{+\infty} C_{lm} L_1^{-l-m} L_2^m \tag{A.7}$$

$$\text{where} \quad L_1 = \ln(-z), \quad L_2 = \ln[-\ln(-z)]\,. \tag{A.8}$$

The coefficients $C_{lm} = (-1)^l \frac{S(l+m,l+1)}{m!}$ are all constants and $S(l+m,l+1)$ is a non-negative Stirling number of the first kind. Now, we apply the asymptotic series expansion in (A.7) to $t_1(\Delta,\delta)$,

$$\begin{aligned} & t_1(\Delta,\delta) \\ = & -\frac{32}{\Delta^2} W_{-1}\left(-\frac{\Delta^2}{128}\sqrt{2\delta}\right) \\ = & \frac{32}{\Delta^2}\left(\ln\left(\frac{128}{\sqrt{2\delta}\Delta^2}\right) + \ln\ln\left(\frac{128}{\sqrt{2\delta}\Delta^2}\right)\right. \\ & \left. -\sum_{l=0}^{+\infty}\sum_{m=1}^{+\infty}(-1)^{l+m} C_{lm} \frac{\left(\ln\ln\left(\frac{128}{\sqrt{2\delta}\Delta^2}\right)\right)^m}{\left(\ln\left(\frac{128}{\sqrt{2\delta}\Delta^2}\right)\right)^{l+m}}\right) \\ \approx & \frac{32}{\Delta^2}\ln\left(\frac{128}{\sqrt{2\delta}\Delta^2}\right)\,. \end{aligned} \tag{A.9}$$

Remark The approximation in step (A.9) follows from

$$\lim_{\delta \to 0^+} \frac{\left(\ln \ln \left(\frac{128}{\sqrt{2\delta}\Delta^2}\right)\right)^m}{\left(\ln \left(\frac{128}{\sqrt{2\delta}\Delta^2}\right)\right)^{l+m}} = 0 \quad \forall\, l \in \mathbb{N}, m \in \mathbb{N}^+. \tag{A.10}$$

Therefore, since we are mostly interested in the case where δ is close to zero, the deletion time $t_1(\Delta, \delta)$ can be approximated by $\frac{32}{\Delta^2} \ln \left(\frac{128}{\sqrt{2\delta}\Delta^2}\right)$.

A.2 M-machine case

Without loss of generality, we assume that machine 1 is the one with the greatest average reward, i.e. $P_1 = \max_i\{P_i\}$. Let T_i denote the deletion time for the i^{th} machine, where $i = 2, \ldots, M$. Clearly, the deletion time of the i^{th} machine should not be longer than the deletion time in the two-machine case where the candidate set is composed of machine 1 and machine i only. Let $\Delta_i = P_1 - P_i$. Following similar steps as in the two-machine case, we derive the following upper bound for T_i.

$$\begin{aligned} T_i &\leq -\frac{32}{\Delta_i^2} W_{-1}\left(-\frac{\Delta_i^2}{64}\sqrt{\frac{\delta}{M}}\right) \\ &\approx \frac{32}{\Delta_i^2} \ln\left(\frac{64}{\Delta_i^2}\sqrt{\frac{M}{\delta}}\right) \qquad \text{(A.11)} \\ &\leq O\left(\frac{\ln\left(\frac{1}{\Delta_i^2}\sqrt{\frac{M}{\delta}}\right)}{\Delta_i^2}\right). \qquad \text{(A.12)} \end{aligned}$$

The approximation in step (A.11) is under the condition of $\sqrt{\frac{M}{\delta}}$ going to infinity.

Now we are able to express an upper bound on the testing complexity of the Successive Deletion Algorithm in the M-machine case. Assuming that $P_1 \geq \cdots \geq P_M$, with probability at least $1 - \delta$, the testing complexity of the Successive Deletion

Algorithm is upper bounded by

$$\begin{aligned}
& \sum_{1}^{M} T_i \\
\leq\ & T_2 + \sum_{2}^{M} T_i \\
\leq\ & O\left(\frac{1}{(P_1 - P_2)^2} \ln\left(\frac{1}{(P_1 - P_2)^2} \sqrt{\frac{M}{\delta}} \right) + \sum_{i=2}^{M} \frac{1}{(P_1 - P_i)^2} \ln\left(\frac{1}{(P_1 - P_i)^2} \sqrt{\frac{M}{\delta}} \right) \right) .
\end{aligned}$$

This is the desired the upper bound in (3.29).

Bibliography

[1] Andrea J. Goldsmith, Pravin P. Varaiya *Capacity of Fading Channels with Channel Side Information.* IEEE Transaction of Information Theory, Vol. 43, NO. 6, November 1997.

[2] I. Emre Telatar, David N. C. Tse. *Capacity and Mutual Information of Wideband Multipath Fading Channels.* IEEE Tran on Information Theory, Vol. 46, No. 4, July 2000.

[3] David N. C. Tse, Pramod Viswanath *Fundamentals of Wireless Communication.* Cambridge University Press, 2005.

[4] H. Robbins. *Some Aspects of the Sequential Design of Experiments.* In Bulletin of the American Mathematical Society, volume 55, pages 527535, 1952.

[5] D.A. Berry and B. Fristedt. *Bandit Problems.* Chapman and Hall, 1985.

[6] Wassily Hoeffding, Probability inequalities for sums of bounded random variables, Journal of the American Statistical Association 58 (301): 1330, March 1963.

[7] P. Auer. N. Cesa-Bianchi, Y. Freund, and R. E. Schapire. *Gambling in a rigged casino: The adversarial multi-armed bandit problem.* In Proc. 36th Annual Symposium on Foundations of Computer Science, pages 322-331. IEEE Computer Society Press. 1995.

[8] E. Even-Dar, S. Mannor and Y. Mansour, *PAC bounds for multi-armed bandit and Markov decision processes*, Fifteenth Annual Conference on Computational Learning Theory, pages 255-270. Springer, 2002.

[9] Shie Mannor and John Tsitsiklis, *The Sample Complexity of Exploration in the Multi-Armed Bandit Problem*, Journal of Machine Learning Research 5 (2004) 623-648.